Magnetic field modeling

using measurements from multiple magnetometers of a motion capture suit

T.A. van Dam

Master of Science Thesis

Delft University of Technology

Delft Center for Systems and Control

Magnetic field modeling

using measurements from multiple magnetometers of a motion capture suit

Master of Science Thesis

For the degree of Master of Science in Systems and Control at Delft University of Technology

T.A. van Dam

June 17, 2025

Faculty of Mechanical Engineering (ME) · Delft University of Technology

Abstract

Ferromagnetic materials in the walls and ground of buildings cause perturbations in the earth's magnetic field. These spatial variations in the ambient magnetic field observed in indoor environments are mostly time-invariant. The deviations of the magnetic field can be captured in a magnetic field map, providing valuable information for indoor localization and navigation. Gaussian processes are a useful tool to model the ambient magnetic field, where the characteristics of the magnetic field are specified by the hyperparameters of the Gaussian process. To avoid the computational difficulties associated with full Gaussian process regression, a reduced-rank approximation is implemented. The magnetic field is measured using a magnetometer. A motion capture suit contains multiple magnetometers, whose relative positions are accurately determined. In this thesis it is researched if the quality of the magnetic field map can be improved when the measurement come from the motion capture suit. This is a challenging task, since the magnetometers are placed at different altitudes and the characteristics of the indoor magnetic field also vary with altitude. Consequently, the hyperparameters that best fit the measurement data are different per magnetometer. The negative effects of this observation are reduced by considering subsets of magnetometers operating at similar altitudes. However, an evident relation between the magnetometer's altitude and its optimal hyperparameters has not been found. The hypothesis that complementing measurements from a single magnetometer with measurements of magnetometers operating at similar altitudes would improve the quality of the magnetic field is not supported based on the experiments. It is expected that either the magnetometer measurements lacked consistency, or that the assumption that the MOCAP suit returned the true magnetometer locations does not apply.

Table of Contents

Preface

My wife has a sports watch to track and analyze her running performance. Although these watches may be costly, valuable information is retrieved from the data provided by these devices. For example, the watch allows one to train based on the heart rate, or one can see the route that has been run. Navigation-related tasks require a GPS connection. My wife is frequently annoyed by the time it takes before the GPS signal is found.

Now I am the one who uses the watch often. Indeed, it is annoying to wait a few minutes just for the device to find the GPS signal, but it helps to know that in indoor environments the GPS signal is blocked by the surroundings. Typically, this problem is easily avoided by first going outside and then letting the device try to make a GPS connection.

The issue that the GPS is blocked in indoor environments does not yield severe problems regarding the sports watch example. However, there are many scenarios in which walking outside is not an option for resolving all difficulties. Especially indoor localization and navigation may be challenging when the GPS signal is unavailable. Therefore, alternative indoor navigation methods, which do not rely on GPS, are important to research. In this thesis a small contribution to this broad and interesting field of research is added.

Acknowledgements

Firstly, I would like to thank my supervisor dr. Manon Kok for introducing me to the amazing research field of sensor fusion and in helping me become a decent engineer. I really appreciate the joy you brought to the meetings. Secondly, I would like to thank Thomas Edridge for his guidance throughout the graduation project. You are a quick thinker, and the meetings were fun with you. To Manon and Thomas, I am glad that you were my supervisors, and I hope you may achieve many more academic milestones in the near future!

I want to thank my friends and family (especially my parents), who supported me during the whole master's program and helped me to stay motivated. And most importantly, I thank my wonderful wife for her countless support, patience, and encouragement.

Delft, University of Technology — T.A. van Dam
June 17, 2025

Chapter 1

Introduction

Indoor positioning plays a crucial role in a wide range of applications, e.g. in robotics, healthcare, security, business and transportation [1]. Indoor locations are challenging environments for a global navigation satellite system (GNSS) to perform well [2]. Various localization methods need additional infrastructure where preliminary installation cannot always be guaranteed [3] or require line-of-sight and may perform poorly in case of fire and smoke [4]. In a building, large spatial variations and small time variations in the ambient magnetic field are typically observed [5,6]. These anomalies contain sufficient information for accurate positioning [7, 8] and possibly orientation [9] and can be captured in a magnetic field map. Because a magnetic field map has the potential to improve indoor localization, methods for magnetic field modeling are an interesting research topic. Nowadays, magnetometers can be produced in unprecedented volumes and at low costs [10], which opens up possibilities for magnetic field mapping using multiple magnetometers. Various authors researched how a magnetic field map is improved by using multiple magnetometers placed on an array [10–15] or on a robot [16]. A motion capture (MOCAP) suit contains magnetometers on different body segments, whose relative positions are accurately determined [17]. Therefore, the MOCAP suit can be viewed as a flexible array. In this thesis, the benefits and challenges of using a MOCAP suit for making magnetic field maps for indoor localization are researched.

This chapter starts with a brief introduction on the relevance of magnetic field maps for indoor localization and on methods that use magnetometer readings to construct a such a map. In the second section the motivation for improving current magnetic field mapping methods using multiple magnetometers is substantiated. It is suggested that a motion capture (MOCAP) suit, in this case a suit equipped with multiple magnetometers, has some promising features to improve the quality of a magnetic field map. Here lies the goal of this thesis: to investigate the benefits and challenges of using multiple magnetometers from a MOCAP suit for magnetic field mapping. The chapter concludes with the organization for the remainder of the report.

1-1 Background

Accurate position determination and navigation tasks play an important role in many applications, e.g. position determination during an emergency, hazardous material transport monitoring, public services optimization and synchronization, position-based advertising, guiding customers in shopping malls, etc. [1, 2]. In outdoor environments GNSS receivers are often used for navigation and positioning tasks [2]. However, for certain indoor applications, such as navigating in a storehouse or hospital, the methods that rely on GNSS signals are subjected to more difficult working conditions, and may perform poorly [2]. Various strategies have been proposed for indoor localization.

1-1-1 Indoor localization

For indoor navigation and positioning applications, sensors that provide accurate position information on a short time-scale (but tend to drift over a longer period) are often combined with absolute position measurements [18]. Well-known examples of sources of these absolute positions are ultrawideband, Wi-Fi, and other technologies that rely on signals-of-opportunity [5,18]. The down-side of such systems is that they suffer from poor localization accuracy when line-of-sight requirements are not met, or that additional (and often expensive) hardware and infrastructure is required to be deployed [5,19]. Under strict line-of-sight requirements vision-based methods, e.g. cameras, and Light Detection and Ranging (LiDAR) are used for accurate positioning strategies [20]. Examples of sensors that are accurate on a short time-scale are the gyroscope and accelerometer in an inertial navigation system (INS) [21]. These systems rely on accurate sensors but suffer from integration drift. The errors in the integration of the measurements from the accelerometer and gyroscope propagate and cause drifting position estimates over longer time-horizons [21]. Magnetometers can be used to reduce the amount of drift [22]. An elaborated survey of indoor localization systems and technologies is presented in [19].

In this research, a localization method that does not require expensive infrastructures or line-of-sight requirements is further researched, namely localization based on the ambient (local) magnetic field. Local magnetic disturbances carry sufficient information for indoor localization using solely magnetometer and accelerometer data when a magnetic field map is available [7]. The magnetic field in a building typically shows large spatial variations and small time variations [5, 6]. Anomalies are induced in the local ambient magnetic field by ferromagnetic materials. The information resulting from distortions in the magnetic field can be exploited to construct a pre-computed map for navigation [6]. Alternatively, the spatial variations are used for simultaneous localization and mapping (SLAM) [18, 22–25], where a map is built and at the same time the position on that map is estimated. Two approaches which are often used for localization using a magnetic field map are by looking for spatial-temporal sequence patterns (matching the magnetometer measurements against a set of fingerprints) and location estimation via sensor fusion (e.g. with a Kalman or particle filter) [16, 26].

1-1-2 Magnetic field mapping

A magnetic field is a mathematical construction used for describing forces induced by magnetic materials and electric currents [6]. As such, on macroscopic scale magnetic fields are vector fields that have a direction and a magnitude at any given location. The earth's magnetic field sets a background for the ambient magnetic field, but deviations and anomalies are caused by the presence of magnetic material in the vicinity of the magnetometer [18,27]. These magnetic materials either give rise to hard iron effects, which are due to the permanent magnetization of the material, or to soft iron effects, which are due to magnetization of the material as a result of an external magnetic field. The magnetic field is measured with a magnetometer, which returns the magnitude of the ambient magnetic field in three directions. In absence of ferromagnetic objects that disturb the measured constant local magnetic field vector, the vector points towards the local magnetic north and thus can be used for heading estimation. In indoor locations, the distortions in the ambient magnetic field, for instance caused by e.g. reinforced concrete and radiators, carry information that can be used for positioning and navigation purposes, when these distortions are regarded as a unique 'fingerprint' to describe the environment [5]. The ambient magnetic field provides valuable information for e.g. indoor positioning because it is temporally stable but shows large spatial variations [18]. A magnetic field map is either made in 2D (a planar map, e.g. [7,16]) or in 3D (e.g. [28,29]).

Each time magnetometers are placed in a different environment, they need (re)calibration [30]. Errors arise from mounting sensors on a magnetic object introduced by soft iron and hard iron effects, non-orthogonality in the three sensor axes, presence of a zero bias null shift (where the sensor measures non-zero values where the magnetic field is zero), and scaling errors (resulting from difference in sensitivity in the three directions for instance) [30–34]. Moreover, the sensor axes are in practice not perfectly aligned when using multiple sensors (e.g. a magnetometer and an inertial measurement unit (IMU)) [30]. Nowadays IMUs are often combined with magnetometers. A multitude of calibration strategies has been proposed to acquire accurate magnetometer measurements that rely on the magnetometer only (e.g. [31–34]) or that rely on the magnetometer in combination with an IMU (e.g. [30]).

It is impossible to measure the magnetic field at each spatial coordinate in the room to find its magnitude. Therefore, an appropriate modeling/interpolation approach is required to construct a useful magnetic field map. Magnetic field mapping amounts to make predictions on the magnitude of the magnetic field at unseen locations based on the magnetometer measurements and/or prior knowledge on the ambient magnetic field. The magnetic field can be modeled by Gaussian processes (GPs) [35]. An advantage of this Bayesian non-parametric probabilistic modeling approach is that prior knowledge on the magnetic field, such as its curl-free properties, could be incorporated [6,18]. In standard Gaussian process regression (GPR) prior knowledge on the process (e.g. the magnetic field) is combined with measurements taken at known inputs (the location of the magnetometers). Besides returning the magnitude of the ambient magnetic field, this method also gives information on the certainty of the estimate, which makes it a suitable tool for the magnetic field mapping task.

1-2 Motivation

The anomalies in the ambient magnetic field at indoor environments contain valuable information for indoor positioning [27]. This calls for methods to obtain accurate and detailed magnetic field maps. GPR seems a suitable method to create such a map. This method omits line-of-sight requirements and additional infrastructure, so that the mapping method can be applied in common indoor environments, such as shopping malls and hospitals, without using a camera or relying on a deployed infrastructure. In this section, the challenges of magnetic field mapping are discussed. Then it is suggested that these challenges are overcome by using the magnetometers from the motion capture (MOCAP) suit for the indoor magnetic field mapping task. This section is concluded by the formulation of the research questions which are answered in this thesis.

1-2-1 Challenges in magnetic field mapping

Two challenges in magnetic field mapping are high-lighted in this thesis. The first challenge concerns the magnetometer location. The benefit of a magnetic field map is that it could be used for indoor localization without additional infrastructure or technologies that require line-of-sight requirements. However, to make a magnetic field map, the absolute position of the magnetometer must be known. Possible solutions to this problem may be found in SLAM [18, 28] or odometry methods [36]. In this research it is used that the MOCAP suit returns accurate absolute estimates [17].

The second challenge is related to the domain of the magnetic field map. The places where the magnetic field must be measured depends on the application of the map. When the map is read by an autonomous vacuum cleaner, it is important to have measurements of the magnetic field close to the ground (where the device operates). On the other hand, when the map is used for navigational purposes of an autonomous drone, likely it is preferred that the map covers areas in a room which are relatively high above the ground. Moreover, the magnetic field map is made by interpolation between the magnetometer measurements, which imposes the requirement that the measurements are not 'too far' away from each other, which may be challenging when it is desired to cover large spaces in a three-dimensional map. It is suggested to perform this interpolation task using GPR. However, GPs are computationally challenging when the training data set is large, and the extend to which predictions can be made on unseen locations based on available measurements from nearby locations is limited [35]. It is observed that ferromagnetic materials in the floor of a building cause the indoor magnetic field to vary with altitude [16]. Hence, the altitude of the magnetometer has an influence on the behavior of the magnetic field that is observed.

1-2-2 Multiple magnetometers

Nowadays, due to the low-cost development of micro-electro-mechanical systems (MEMS) in unprecedented volumes, sensors such as accelerometers, gyroscopes, and magnetometers, are widely available with a high performance-to-price ratio [10]. This opens up the field for sensor fusion, where multiple sensors are used to improve, in this case, the ambient magnetic field. Some examples of sensor fusion have already been introduced in this chapter, for instance the combination between sensors that are accurate on a short time-scale, but drift over time, and measurements from absolute position technologies, to provide accurate position estimates.

A method to solve the problem of accurate localization using sensor fusion (and without line-of-sight requirements and additional infrastructure) is presented by Viset *et al.* [22]. They propose a method to limit the integration drift using foot-mounted sensors (IMU and magnetometer) using a zero velocity update-aided extended Kalman filter (ZUPT-aided EKF), where the information that the stance phase of the foot provides is exploited. The remaining drift is removed using magnetic field simultaneous localization and mapping (SLAM), where a magnetic field map is made and at the same time the position on this map is estimated using a Rao-Blackwellized particle filter [22].

Regarding the challenge of obtaining sufficient magnetometer data in a large spatial area to create a detailed magnetic field map, several solutions that build upon sensor fusion are found in literature. Viset *et al.* [37] present a method for distributed multi-agent magnetic field norm SLAM, where multiple agents are utilized. Using multiple magnetometers at the same time allows increasing the speed at which the measurements of the magnitude of the magnetic field are collected. Other options to use multiple magnetometers at the same time are by measuring the magnetic field using an array of magnetometers [10, 11, 13–15] or a MOCAP suit [17].

Instead of using a single sensor and using the stable characteristics of the magnetic field, Skog *et al.* [15] use an array of magnetometers to take an image-like measurement of a vector field. A magnetic field map is constructed with the measurements, where an odometry process is implemented such that the pose change of the array with the smallest prediction error is calculated [15]. In presence of magnetized object, their method reduces the navigation error growth in an INS. Edridge and Kok [11] use the information that the relative positions between the sensors are known, but the position of the array itself is uncertain, to improve the magnetic field map quality.

The size of these magnetometer arrays can vary. A miniaturized sensor array where the sensors are distributed over a square with a side of approximately 2 cm is used in [10, 13]. However, in [13], by visual inspection, it is pointed out that the field variations in the magnetic field inside an office building can well be approximated with a length scale of approximately 0.5 m. Therefore, the magnetometers would preferably be distributed over a larger square with sides of a few decimeters. A larger array is used in [11, 14, 15], with a size slightly larger than 0.3 m $\times$ 0.2 m.

Yet another configuration with multiple magnetometers is presented by [16]. A wheeled mobile robot is equipped with 25 magnetometers from ankle height to head height. The advantage of their setup is that the influence of the height of the magnetometer can be examined for localization and mapping. Hanley *et al.* [16] point out that the assumption that the indoor magnetic field does not vary with height is likely to be violated.

1-2-3 Introduction to the MOCAP suit

The MOCAP suit can also be seen as an array, where the magnetometers are placed on different body parts. Consequently, the magnetometers can move with respect to each other. Moreover, the distances between the magnetometers are significantly larger than those of the arrays discussed in the former section. The suit described in [17] contains seventeen sensors (each consisting of an IMU and a magnetometer). Their measurements are synchronized. The relative positions between the body segments are known due to biomechanical constraints integrated in the software of the suit [17]. Contact detection allows to accurately predict the altitude (with respect to the floor) of the complete assembly of the body segments. When the suit is used to map the ambient magnetic field in an indoor environment, a similar approach as Edridge and Kok [11] could be applied to improve the map quality. The position estimation of the suit is subjected to drift, coming from the integration of the noisy accelerometer measurements to obtain the absolute position of the suit [17]. However, the position estimates are continuously corrected in a sensor fusion scheme, which reduces the drift [17]. Unbound drift can be avoided by using the magnetometer measurements [17]. Contrary to the magnetometer array, the magnetometers are not rigidly attached to a platform. Moreover, the sensors are placed in a three-dimensional configuration (and not on a flat platform), where sensors range from foot-height to head-height. Veen [38] used a MOCAP suit for SLAM, but suggested that the mapping part may be improved by further research on the fusion of the magnetometer measurements. The suit has also been used to for making large-scale magnetic field maps for indoor environments [39]. The authors of [39] used a single sensor from the suit to obtain the measurements.

1-2-4 Research goal

The MOCAP suit, with its high magnetometer quality and accurate estimations of the relative positions of the body segments, is a promising tool for making magnetic field maps. Seventeen magnetometers are placed on different body segments, and operate therefore at different altitudes. Considering the observation that the anomalies in the ambient magnetic field are caused by ferromagnetic materials in the floor and walls, it is expected that the characteristics of the magnetic field change within the indoor environment. Indoor localization is enabled by the anomalies in the ambient magnetic field, thus if the map is used for indoor localization, it must capture these spatial variations. Since the suit accurately determines the height of the body segments, the interest in this research mostly lies in the relation between the magnetometer altitude and the magnetometers used for modeling the magnetic field with Gaussian processes. When multiple magnetometers are used, the magnetic field measurements differ more because of the height difference than when less magnetometers are used at the cost of including less information in the making of the magnetic field map. The question arises how modeling the magnetic field with a combination of magnetometers influences the quality of a 3D magnetic field map. Consequently, the research question in this report is formulated as:

What are the benefits and challenges of using multiple magnetometers from a motion capture suit to model the ambient magnetic field in indoor environments?

The hypothesis is that the magnetic field map has a higher quality when a subset of magnetometers sharing approximately the same altitude is used for modeling, compared to the case where either a single magnetometer is used or all magnetometers are used. It is expected that the predictions at the test locations of a single magnetometer are improved by complementing the data of this magnetometer with magnetometer data from neighboring magnetometers because more information on the magnetic field in close proximity of the magnetometer is utilized. On the other hand, the subset of magnetometers is also expected to improve the quality of the magnetic field map compared to the scenario where all seventeen magnetometers of the MOCAP suit are used. The anomalies in the magnetic field change with altitude [16], and therefore it is expected that the magnetic field observed by the magnetometers with the largest altitude differs significantly from the magnetic field observed at the feet. It is expected that the underlying characteristics of the magnetic field observed at each body segment are too diverse to be captured in a magnetic field model using all seventeen magnetometers simultaneously. The data from a subset of magnetometers operating at similar altitudes is expected to show strong resemblance between the magnetic field measurements, allowing for a better magnetic field map compared to the case where seventeen magnetometers are used.

To validate the hypothesis and to fully answer the research question, three sub-questions are formulated.

The first sub-question regards the task of modeling the ambient magnetic field of an indoor environment. Gaussian processes are regularly applied for the magnetic field mapping (e.g. [18]). The MOCAP suit returns accurate locations of the body segments. It is desired to include this information in the model. Moreover, the modeling method must deal with large amounts of data, since multiple magnetometers with high sampling rates are available. The first sub-question is formulated as:

How can multiple magnetometers of the motion capture suit be combined to model the ambient magnetic field in indoor environments?

The second sub-question concerns the spatial variations of the magnetic field. Before performing GPR, the behavior and the characteristics of the ambient magnetic field at the indoor experiment site are inspected based on the measurements from the MOCAP suit. Specifically, the influence of the proximity of the ferromagnetic disturbances in the floor and in the walls to the magnetometers are scrutinized. It is expected that the magnetic field varies with altitude as a result of the ferromagnetic materials in the floor, because this has been observed in literature [16]. However, the influence of the walls may also be observed in the experiments. Hence, the second sub-question is formulated as:

How do spatial variations in the ambient magnetic field change in an indoor environment and what is the influence of the proximity of magnetic field disturbing sources on the spatial variations?

The Xsens MVN Link MOCAP suit contains seventeen magnetometers. Principally, the advantage of using multiple magnetometers for magnetic field mapping is that more information on the magnetic field is available. However, challenges arise when measurements must be combined where the underlying characteristics of the magnetic field observed by the magnetometers significantly differ between the magnetometers. This is likely the case for the MOCAP suit, since the magnetometers are placed on different body segments operating at different altitudes. During the experiment several magnetometer combinations are made. Under the assumption that the magnetic field varies with the altitude, magnetometer subsets are created based on the altitude of the magnetometers. The first option is to include data of many magnetometers in a subset to inform the model with many measurements at different locations in the indoor room. However, with the increase in the range of heights, also an increase in the range of optimal hyperparameters is expected, which possibly complicates accurate modeling of all used data. Alternatively, data from magnetometers in a small range of heights are collected in a subset, such that the optimal hyperparameters of these magnetometers are close. However, less information of the magnetic field is included.

Moreover, the influence of moving in the MOCAP suit is investigated. The magnetometers of the MOCAP suit are not attached to a rigid array such as [10,11,15]. Instead, by moving with different walking methods, the relative distances between the magnetometers are alternated. Consequently, the composition of magnetometers in a certain range of heights, and therewith in a certain subset, are affected by the walking method. In this research, walking methods are chosen where the individual magnetometers remain approximately at a single altitude during an experiment. This way it is likely that the data of an individual magnetometer can be described accurately by a single set of hyperparameters. However, it must be verified that this assumption is not invalid due to the presence of the ferromagnetic materials in the walls around the experiment site. Finally, the last sub-question is formulated as:

What are the benefits and challenges of combining multiple magnetometers of the motion capture suit to create a 3D magnetic field map of an indoor environment?

1-3 Organization

The remainder of this thesis is structured as follows. Firstly, Chapter 2 is dedicated to magnetic field modeling, specifically focusing on Gaussian processes. To avoid the computational pitfalls associated to Gaussian processes, an approximation method is presented. It is proposed to model the magnetic field using the magnetometer measurements from a motion capture suit. In Chapter 3 the assumptions for the model are substantiated and the performance and limitations of magnetic field mapping with the MOCAP suit are examined based on experiments. In these experiments, it is examined if the observations on the magnetic field agree with literature. Magnetometer data are combined to include more information about the magnetic field in the model. Then the influence of the way of movement in the motion capture suit on combining magnetometer data and on the magnetic field map quality is researched. In Chapter 4, the results are discussed. Lastly, conclusions are drawn and recommendations are made in Chapter 5.

Chapter 2

Magnetic field modeling using GPs and a motion capture suit

The aim of this chapter is to research how multiple magnetometers from the MOCAP suit are used to model the magnetic field. To this end, predictions about the magnetic field magnitude at locations where no measurement is taken are made. The interest lies in creating a magnetic field map which can be utilized for indoor localization. A modeling approach is required which captures the spatial variations of the magnetic field. Gaussian processes are a suitable tool for this task and literature presents a wide variety of options modeling the ambient magnetic field using GP's (e.g. [11, 18, 22, 23, 28, 29, 40]).

A brief introduction to Gaussian process regression (GPR) is presented in this chapter. The chapter starts with introducing the coordinate frames of the MOCAP suit in Section 2-1. Section 2-2 explains how GP's are used for modeling a system and how good values for the modeling parameters, known as the hyperparameters, are obtained. In Section 2-3 a reduced-rank approximation is introduced, which avoid the computational demands associated with Gaussian processes. In Section 2-4 is discussed how to model the magnetic field with a MOCAP suit equipped with multiple magnetometers. Lastly, some performance metrics to evaluate the quality of the magnetic field map are discussed in Section 2-5.

2-1 Coordinate frames

The primary interest in this work is the modeling of the indoor magnetic field based on measurements from the magnetometers on a MOCAP suit. The MOCAP suit can be considered as an assembly of multiple body segments. Using the suit, the relative positions of these body segments are accurately determined. Information on the absolute position of the assembly of the body segments in an indoor environment is required to make a magnetic field map of this location. The following coordinate frames are introduced:

- navigation frame n is the coordinate frame of the body frame at time zero. The negative z-axis aligns with the gravity field, following [41]. Sometimes this frame is referred to in literature as world or global frame.
- body frame b_i is the coordinate frame where the axes are aligned with the i-th body segment.
- sensor frame s_j is the coordinate frame that aligns with the j-th sensor axes.

Note that a MOCAP suit contains multiple body and sensor frames. It is assumed that for each sensor frame there is a body frame it aligns and coincides with. The magnetometer measurements are the magnitude of the magnetic field components in the sensor frame, s. In the context of magnetic field mapping, it is desired to express all magnetometer readings in the navigation frame, n. Each magnetometer measurement at time step k is therefore mapped to the navigation frame using

$$\mathbf{y}_k^{\mathrm{n}} = \mathbf{R}_k^{\mathrm{ns}} \mathbf{y}_k^{\mathrm{s}}, \tag{2-1}$$

where $\mathbf{R}_k^{\mathrm{ns}}$ is the k-th rotation matrix in which the superscript ns denotes the rotation from the sensor frame s to the navigation frame n. The focus in this research is on magnetic field mapping and it is assumed that the true magnetometer locations are returned by the MOCAP suit. Since all measurements and sensor locations are expressed in the navigation frame the superscripts omitted for legibility. Moreover, in this section the magnetometers are assumed to be calibrated properly (e.g. see [30]).

2-2 Gaussian process regression

The problem of learning input-output mappings from empirical data is, for continuous outputs, known as regression [35]. Gaussian process regression (GPR) is an effective tool to make predictions on the outcome of a system, where information from measurement data and prior knowledge can be incorporated in a Bayesian manner [35]. In the context of magnetic field mapping the empirical data come from magnetometers. Rasmussen and Williams [35] define a Gaussian process (GP), in particular in the context of regression, as a collection of random variables, any finite number of which have a joint Gaussian distribution. Even when merely considering Gaussian processes to model the ambient magnetic field a variety of design choices remain. In this section it is explained what modeling approaches using Gaussian processes are suitable to make a magnetic field map for indoor localization.

One of the strengths of the GP model is that the model is non-parametric, resulting in some flexibility in the model fit [35]. Instead of providing a single 'best-fit' to the observed data, a complete posterior distribution over functions is provided [42]. A GP is the extension of the Gaussian distribution to functions [42]. It is defined as a collection of random variables, any finite number of which have a joint Gaussian distribution [35]. Rasmussen and Williams [35] note that the definition of a GP automatically implies a consistency requirement. The consistency requirement, a.k.a. the marginalization property, implied by the Gaussian process model yields that the examination of a larger set of data points does not change the distribution of the smaller set [35]. This section concerns how GP's are used to make predictions based on the measurements of a single sensor.

2-2-1 Gaussian process regression with a single sensor

GPR is a useful tool for making predictions on the outcome of a system based on prior knowledge on the behavior of the system and measurement data. The formulation of Rasmussen and Williams [35] is that in GPR inferences about the relationship between inputs and outputs (a.k.a. targets) are made. Not only a predicted value is obtained in GPR, but also information on the certainty of the prediction. The measurement data consists of in- and output pairs. This dataset is split in a train and a test dataset. Firstly, n observations are collected in the train dataset $\mathcal{D} = \{(\mathbf{x}_k, y_k) | k = 1, 2, \ldots, n\}$. This data is used to 'fit' the GP. Similarly, $n_\star$ different in- and output pairs are put in the test dataset. This dataset is used to make predictions at 'unseen' locations and to evaluate performance of the GP.

The GP takes a d-dimensional input $\mathbf{x} \in \mathbb{R}^d$ to return a p-dimensional latent output $f(\mathbf{x}) \in \mathbb{R}^p$. A GP is specified by its mean function $m(\mathbf{x})$ and its covariance function $\kappa(\mathbf{x}, \mathbf{x}')$, also referred to as the kernel function. The characteristics and prior knowledge on the behavior of the system are incorporated in these functions.

Consider the task of magnetic field mapping using GPR. One is interested in making predictions on the magnetic field based on prior knowledge on the properties of the ambient magnetic field and based on magnetometer data. In this case the input is the magnetometer location, which is expressed as the spatial coordinate $\mathbf{x}_k \in \mathbb{R}^3$, where k indicates the time-step. The magnitude (norm) of the magnetic field y_k is taken as its corresponding output. This particular choice for the output is a scalar value, but the GPR framework works for multidimensional outputs too. In real-world systems the latent outputs of the magnetometer are not available due to measurement noise. This measurement noise is modeled as additive independent and identically distributed (i.i.d.) Gaussian noise, e.g. similar to [11, 18]. Consequently, the following model is formulated:

$$\begin{aligned} f(\mathbf{x}) &\sim \mathcal{GP}\left(m(\mathbf{x}), \kappa(\mathbf{x}, \mathbf{x}')\right), \\ y_k &= f(\mathbf{x}_k) + e_{\mathrm{y},k}, \end{aligned} \tag{2-2}$$

where the measurement noise $e_{\mathrm{y},k} \sim \mathcal{N}(0, \sigma_{\mathrm{y}}^2)$ is zero-mean white noise (ZMWN) with the measurement noise variance σ_{y}^2.

The mean function $m(\mathbf{x})$ is used to capture the characteristics of the underlying constant magnetic field, whereas the covariance function captures the anomalies and perturbations of this field. In this work the mean function is modeled as a zero-mean function $m(\mathbf{x}) = 0$ because the characteristics of the magnetic field can be fully captured by the kernel function (see e.g. [18]). The n training inputs are aggregated in the vector $\mathbf{X}_{1:n} = [\mathbf{x}_1^\top, \mathbf{x}_2^\top, \ldots, \mathbf{x}_n^\top]^\top \in \mathbb{R}^{3n}$ (and $\mathbf{X}'_{1:n}$ is similarly defined) such that the kernel matrix $k(\cdot, \cdot)$ is evaluated at all input pairs $(\mathbf{x}, \mathbf{x}')$ as

$$k(\mathbf{X}_{1:n}, \mathbf{X}'_{1:n}) = \begin{bmatrix} \kappa(\mathbf{x}_1, \mathbf{x}'_1) & \kappa(\mathbf{x}_1, \mathbf{x}'_2) & \ldots & \kappa(\mathbf{x}_1, \mathbf{x}'_n) \\ \kappa(\mathbf{x}_2, \mathbf{x}'_1) & \kappa(\mathbf{x}_2, \mathbf{x}'_2) & \ldots & \kappa(\mathbf{x}_2, \mathbf{x}'_n) \\ \vdots & \vdots & \ddots & \vdots \\ \kappa(\mathbf{x}_n, \mathbf{x}'_1) & \kappa(\mathbf{x}_n, \mathbf{x}'_2) & \ldots & \kappa(\mathbf{x}_n, \mathbf{x}'_n) \end{bmatrix}. \tag{2-3}$$

The kernel for the train data is compactly written as $\mathbf{K} \triangleq k(\mathbf{X}_{1:n}, \mathbf{X}_{1:n}) \in \mathbb{R}^{n \times n}$. This kernel matrix is used to incorporate the knowledge on how the system is expected to 'behave'. Before observing or using any measurements, information on the system is specified through the prior as

$$p(\mathbf{f}_{1:n}|\mathbf{X}_{1:n}, \boldsymbol{\theta}) = \mathcal{N}(\mathbf{0}_n, \mathbf{K}), \tag{2-4}$$

with the latent function values $\mathbf{f}_{1:n} \triangleq [f(\mathbf{x}_1), f(\mathbf{x}_2), \ldots, f(\mathbf{x}_n)]^\top \in \mathbb{R}^n$ and $\mathbf{0}_n \in \mathbb{R}^n$ denoting a vector of zeros. The parameters that define the characteristics of the kernel function are called the hyperparameters $\boldsymbol{\theta}$. The specification of the kernel implies a distribution over functions [35], and thus samples can be drawn from this distribution at any number of points. The magnetic field magnitude is predicted at a location where no measurement is taken. This location is named the test point $\mathbf{x}_\star$. The posterior distribution over functions that 'agree' with the training data is obtained by conditioning the joint Gaussian prior distribution on the observations [35]. To formulate the joint distribution of the noisy magnetometer data and the function values $f_\star \triangleq f(\mathbf{x}_\star)$ that comply with the prior the following kernel matrices are defined: $\mathbf{k}_\star \triangleq k(\mathbf{X}_{1:n}, \mathbf{x}_\star) \in \mathbb{R}^n$, $\mathbf{k}_\star^\top \triangleq k(\mathbf{x}_\star, \mathbf{X}_{1:n}) \in \mathbb{R}^{1\times n}$, and $k_{\star\star} \triangleq k(\mathbf{x}_\star, \mathbf{x}_\star) \in \mathbb{R}$. Consequently, the joint distribution is written as

$$\begin{bmatrix} f_\star \\ \mathbf{y}_{1:n} \end{bmatrix} \sim \mathcal{N}\left(\begin{bmatrix} 0 \\ \mathbf{0}_n \end{bmatrix}, \begin{bmatrix} k_{\star\star} & \mathbf{k}_\star^\top \\ \mathbf{k}_\star & \mathbf{K} + \sigma_{\mathrm{y}}^2 \mathcal{I}_n \end{bmatrix} \right). \tag{2-5}$$

Following Rasmussen and Williams [35], the predictive equations now can be written, compactly shown by defining $\mathbb{E}[f_\star] \triangleq \mathbb{E}[f_\star|\mathbf{X}_{1:N}, \mathbf{y}_{1:N}, \mathbf{x}_\star, \boldsymbol{\theta}]$ and $\mathbb{V}[f_\star] \triangleq \mathbb{V}[f_\star|\mathbf{X}_{1:N}, \mathbf{y}_{1:N}, \mathbf{x}_\star, \boldsymbol{\theta}]$, as

$$\begin{aligned} \mathbb{E}[f_\star] &= \mathbf{k}_\star^\top \left(\mathbf{K} + \sigma_{\mathrm{y}}^2 \mathcal{I}_n\right)^{-1} \mathbf{y}, \\ \mathbb{V}[f_\star] &= k_{\star\star} - \mathbf{k}_\star^\top \left(\mathbf{K} + \sigma_{\mathrm{y}}^2 \mathcal{I}_n\right)^{-1} \mathbf{k}_\star. \end{aligned} \tag{2-6}$$

The predictive mean function returns the predicted value of the modeled system at the test location $\mathbf{x}_\star$. Moreover, the predictive variance function yields information about the certainty of the prediction. This variance will be lower when a test point is close (in space) to a training point, but it will be larger when all training points are further away.

2-2-2 Magnetic field model

The criteria for a good magnetic field map depend on the application for the map. When a magnetic field map is used for indoor navigation, the unique fingerprints of the map are used to determine the user's position. Hence, the emphasis is on capturing the spatial variations of the magnetic field. Literature provides numerous options when it comes to this task. Solin *et al.* [18] consider the three dimensional magnetic field measurements from the magnetometer. Two different interpolation methods that rely on GPs are presented in their work. The first method regards the separate modeling of the magnetic field components, where the magnetic field measurements are modeled as realizations of three independent GP priors with shared hyperparameters, resulting in a flexible model with conservative assumptions [18]. In the second method of Solin *et al.* is not presented here, but then the magnetic field is modeled as the gradient of a scalar potential, which allows to incorporate physical knowledge of the magnetic field characteristics [18]. Contrary to considering the three components of the magnetic field, some maps are made using the magnitude (or norm) of the magnetic field (e.g. [11, 39]), which is also done in this work.

As mentioned in Section 2-2-1, the constant mean of the magnetic field can be modeled as a part of the kernel, resulting in the model

$$\begin{aligned} f(\mathbf{x}) &\sim \mathcal{GP}\left(0, \kappa(\mathbf{x}, \mathbf{x}')\right), \\ y_k &= f(\mathbf{x}_k) + e_{\mathrm{y},k}, \end{aligned} \tag{2-7}$$

where y_k is the magnetic field magnitude measurement corrupted by Gaussian noise. The characteristics of the magnetic field are modeled in the kernel as

$$\kappa(\mathbf{x}, \mathbf{x}') = \kappa_{\mathrm{const.}}(\mathbf{x}, \mathbf{x}') + \kappa_{\mathrm{SE}}(\mathbf{x}, \mathbf{x}'), \tag{2-8}$$

with

$$\kappa_{\mathrm{const.}}(\mathbf{x}, \mathbf{x}') = \sigma^2_{\mathrm{const.}}, \tag{2-9}$$

$$\kappa_{\mathrm{SE}}(\mathbf{x}, \mathbf{x}') = \sigma^2_{\mathrm{SE}} \exp\left(-\frac{||\mathbf{x} - \mathbf{x}'||^2}{2\ell^2_{\mathrm{SE}}}\right). \tag{2-10}$$

The earth magnetic field is disturbed by ferromagnetic materials in indoor environments. Hence when a magnetic field map is made of an indoor location, the earth magnetic field is perturbed. The earth magnetic field is modeled by a constant term in the kernel $\kappa_{\mathrm{const.}}(\cdot, \cdot)$. It contains one hyperparameter $\sigma_{\mathrm{const.}}$ which describes the size of the underlying magnetic field. The anomalies/perturbations are captured by the second part of the covariance function. This kernel is called the squared-exponential (SE) kernel, $\kappa_{\mathrm{SE}}(\cdot, \cdot)$, which is used in many magnetic field mapping applications to capture the spatial variations (e.g. [18]). It has two hyperparameters.

The anomalies of the magnetic field are the feature which is exploited for indoor navigation using magnetic field maps. Therefore, in this research the primary interest lies in capturing these spatial variations. Alternatively to modeling the mean of the magnetic field using a constant kernel, the mean of the training data measurements is subtracted from all measurements. Consequently, the constant part in Eq. (2-8) disappears and merely the anomalies are captured, using the SE kernel in Eq. (2-10) as

$$\kappa(\mathbf{x}, \mathbf{x}') = \kappa_{\mathrm{SE}}(\mathbf{x}, \mathbf{x}'). \tag{2-11}$$

The approach where the mean is removed from the magnetic field measurements is used in the remainder of this research.

2-2-3 Hyperparameter training

In this section a brief explanation is given about how good values for the hyperparameters $\boldsymbol{\theta}$ are obtained, without discussing the particular model choices for magnetic field mapping. A non-Bayesian approach in the form of optimization of the marginal likelihood is followed to find the optimal hyperparameter values [42]. An important aspect of selecting the hyperparameters is that these result in a good model fit over the data, and that under- or overfitting is avoided. The kernel for the magnetic field mapping task and the physical interpretation of the hyperparameters are discussed in Section 2-2-2.

The optimization of the marginal likelihood is recast as a minimization problem of the negative log marginal likelihood (NLML). Optimizing the log marginal likelihood with respect to the hyperparameters $\boldsymbol{\theta}$ should give the optimal values for the hyperparameters. However, there is no guarantee for optimal values because the NLML is a highly nonlinear function and therefore only a local minimum is obtained by the optimization. The matrix $\mathbf{Q} = \mathbf{K} + \sigma_{\mathrm{y}}^2 \mathcal{I}$ is defined for a shorthand notation. Rasmussen [35] define the NLML as

$$\mathcal{L}(\boldsymbol{\theta}) = -\log p(\mathbf{y}|\mathbf{X}, \boldsymbol{\theta}) = \frac{1}{2}\log|\mathbf{Q}| + \frac{1}{2}\mathbf{y}^\top \mathbf{Q}^{-1}\mathbf{y} + \frac{n}{2}\log 2\pi, \tag{2-12}$$

and they point out that the three terms respectively represent the complexity penalty, the data-fit, and the normalization constant. The analytical gradient is

$$\frac{\partial \mathcal{L}(\boldsymbol{\theta})}{\partial \theta_j} = \frac{1}{2}\mathrm{tr}\left(\mathbf{Q}^{-1}\frac{\partial \mathbf{Q}}{\partial \theta_j}\right) - \frac{1}{2}\mathbf{y}^\top \mathbf{Q}^{-1}\frac{\partial \mathbf{Q}}{\partial \theta_j}\mathbf{Q}^{-1}\mathbf{y}, \tag{2-13}$$

which enables efficient gradient-based optimization methods such as the Broyden-Fletcher-Goldfarb-Shanno (BFGS) algorithm [6].

2-3 Reduced-rank approximation

One of the pitfalls associated with GPs, is their computational complexity. When the number of data grows large the inversion of the matrix is an $\mathcal{O}(n^3)$ operation and the memory requirements scale as $\mathcal{O}(n^2)$ [43]. In Section 2-4 the number of data will grow large since a MOCAP suit with seventeen magnetometers with high sampling rates is used to measure the magnetic field. Solin and Särkkä [43] propose a reduced-rank approximation for the covariance function. They use n_b basis functions to approximate the kernel, resulting in a reduction of both the computational complexity and memory requirements when $n_b < n$, which become respectively $\mathcal{O}(n_b^2 n)$ and $\mathcal{O}(n_b n)$ [18, 43]. Solin and Särkkä [43] present a method to obtain approximate eigendecompositions of covariance functions in terms of an eigenfunction expansion of the Laplace operator in a compacts subset of $\mathbb{R}^d$. The covariance function is interpreted as the kernel of a pseudo-differential operator and approximated using Hilbert space methods [43]. The reduced-rank approximation presented by Solin and Särkkä [43] is regularly used for modeling the magnetic field as the gradient of a scalar potential [18, 38, 41]. In this research the method is used for modeling the norm of the magnetic field.

2-3-1 Hilbert-space method

Solin and Särkkä [43] present a reduced-rank method which avoids computational difficulties of full GPR, arising when large kernel matrices must be inverted, by introducing an approximation for stationary and isotropic covariance functions. In their work, a Hilbert-space approximation for the pseudo-differential operator is formed, which they define as a series of Laplace operators. They define a compact set $\Omega \subset \mathbb{R}^d$ and consider the eigenvalue problem for the Laplace operators with Dirichlet boundary conditions [43], written as

$$\begin{cases} -\nabla^2 \phi_j(\mathbf{x}) = \lambda_j^2 \phi_j(\mathbf{x}), & \mathbf{x} \in \Omega, \\ \quad\;\; \phi_j(\mathbf{x}) = 0, & \mathbf{x} \in \partial\Omega, \end{cases} \tag{2-14}$$

where $\phi_j(\mathbf{x})$ denotes the j-th basisfunction and λ_j is the j-th eigenvalue of the Laplace operator with $j = \{1, 2, \ldots, n_b\}$ [18, 43]. Considering the aim to make a magnetic field map, it is sensible to model the magnetic field in subsets of $\mathbb{R}^3$, and thus the example of Solin *et al.* [18] is followed by restricting the scope to domains Ω comprising three-dimensional cuboids. However, in this work the formulation of Viset *et al.* [41] is used, and the domain is defined as $\Omega = [L_{l,1}, L_{u,1}] \times [L_{l,2}, L_{u,2}] \times [L_{l,3}, L_{u,3}]$, where l and u stand for lower and upper respectively to define the dimensions of the domain in each direction. In this work a single domain is considered. However, for large domains the domain can be divided into smaller tiles to reduce the computational complexity [28,38,39]. The domain definition is not limited to cuboids and may also be formulated as e.g. hexagons [28]. By suitably choosing Ω the model reverts back to the prior outside the region of the observed data for regression problems with a stationary covariance function [18]. The covariance function in Eq. (2-11) to model the magnetic field is both stationary and isotropic, fulfilling the requirements to approximate it using Hilbert space methods [43]. Proceeding with the approach of Solin *et al.* [18] the covariance function is now approximated as

$$\begin{aligned}\kappa(\mathbf{x}, \mathbf{x}') &= \kappa_{\text{SE}}(\mathbf{x}, \mathbf{x}') \\ &\approx \sum_{j=1}^{n_b} S_{\text{SE}}(\lambda_j)\phi_j(\mathbf{x})\phi_j(\mathbf{x}').\end{aligned} \tag{2-15}$$

The approximated covariance function is stationary and thus the approximation is based on a truncated series where $S_{\text{SE}}(\cdot)$ is the spectral density function of the Gaussian process (specifically the squared exponential covariance function) [18, 43]. Respectively, the basis functions and the corresponding eigenvalues are defined based on the work of Viset *et al.* [41] which gives

$$\phi_j(\mathbf{x}) = \prod_{d=1}^{3} \frac{\sqrt{2}}{\sqrt{L_{u,d} - L_{l,d}}} \sin\left(\frac{\pi n_{j,d}(x_d + L_{l,d})}{L_{u,d} - L_{l,d}}\right), \tag{2-16}$$

$$\lambda_j^2 = \sum_{d=1}^{3} \left(\frac{\pi n_{j,d}}{L_{u,d} - L_{l,d}}\right)^2, \tag{2-17}$$

where $n_{j,d}$ denotes an entry from the matrix $\mathbf{n} \in \mathbb{R}^{n_b \times 3}$ which consists of an index set of permutations of integers $\{1, 2, \ldots, n_b\}$ [18]. Note that the basisfunctions only are required to be evaluated once, because they are independent of the hyperparameters [18]. Through the projection of the process $\varphi(\cdot)$ to a truncated set of n_b basis functions of the Laplacian in Eq. (2-15) the Solin and Särkkä [43] approximate the process as

$$\varphi(\mathbf{x}) \approx \sum_{j=1}^{n_b} w_j \phi_j(\mathbf{x}), \tag{2-18}$$

where $w_j \sim \mathcal{N}\left(0, S_{\text{SE}}(\sqrt{\lambda_j})\right)$ is regarded as the j-th weight for the corresponding basis function. The spectral density for the squared exponential covariance function in Eq. (2-11) is formulated by Solin *et al.* [18] as

$$S_{\text{SE}}(\omega) = \sigma_{\text{SE}}^2 \left(2\pi\ell_{\text{SE}}^2\right)^{\frac{3}{2}} \exp\left(-\frac{\omega^2 \ell_{\text{SE}}^2}{2}\right), \tag{2-19}$$

where σ_{SE}^2 and ℓ_{SE}^2 are the same hyperparameters as those introduced in previous section. Following the approach in [18, 41], Eq. (2-16) is written in matrix format by placing the weights in a vector and collecting the basis functions in a matrix $\mathbf{\Phi}_{1:n} \in \mathbb{R}^{n \times n_b}$ with the rows

$$\mathbf{\Phi}_k = (\phi_1(\mathbf{x}_k), \phi_2(\mathbf{x}_k), \ldots, \phi_{n_b}(\mathbf{x}_k)) \,. \tag{2-20}$$

When the weights from Eq. (2-18) are placed in the vector $\mathbf{w} = [w_1, w_2, \ldots, w_{n_b}]^\top$, the equation is written in vector format, following [18, 41], as

$$\varphi(\mathbf{x}) \approx \mathbf{\Phi}\mathbf{w}. \tag{2-21}$$

As shown in [18, 41], the weights have the prior distribution

$$\mathbf{w} \sim \mathcal{N}(\mathbf{0}, \mathbf{\Lambda}) \tag{2-22}$$

where $\mathbf{\Lambda}$ is the diagonal matrix of the leading n_b approximate eigenvalues [43] which is defined similar to [18, 41] as

$$\mathbf{\Lambda} = \operatorname{diag}\left(S_{\mathrm{SE}}(\lambda_1), S_{\mathrm{SE}}(\lambda_2), \ldots, S_{\mathrm{SE}}(\lambda_{n_b})\right). \tag{2-23}$$

A method to determine the number of basis functions based on experiment data is shown in Viset *et al.* [41]. The matrix which collects the basis functions for the test point $\phi_\star \in \mathbb{R}^{1 \times n_b}$, is defined similar to Eq. (2-20). Let the remaining kernel matrices of Section 2-2-1 be approximated as $\mathbf{k}_\star \approx \mathbf{\Phi}_{1:n}\mathbf{\Lambda}\phi_\star^\top$, $\mathbf{k}_\star^\top \approx \phi_\star\mathbf{\Lambda}\mathbf{\Phi}_{1:n}^\top$, and $k_{\star\star} \approx \phi_\star\mathbf{\Lambda}\phi_\star^\top$. The predictive equations in Eq. (2-6) are then, following [43], approximated as

$$\begin{aligned}\mathbb{E}[f_\star] &\approx \phi_\star \left(\mathbf{\Phi}_{1:n}^\top\mathbf{\Phi}_{1:n} + \sigma_{\mathrm{y}}^2\mathbf{\Lambda}^{-1}\right)^{-1}\mathbf{\Phi}_{1:n}^\top\mathbf{Y}_{1:n},\\ \mathbb{V}[f_\star] &\approx \sigma_{\mathrm{y}}^2\phi_\star\left(\mathbf{\Phi}_{1:n}^\top\mathbf{\Phi}_{1:n} + \sigma_{\mathrm{y}}^2\mathbf{\Lambda}^{-1}\right)^{-1}\mathbf{\Phi}_{1:n}^\top.\end{aligned} \tag{2-24}$$

Until now, only a single test location is considered. However, in many practical applications, e.g. making a magnetic field map, predictions at multiple locations are required. Therefore, the number of test locations is increased similar to the train locations. The vector containing the basis functions for the single test location $\phi_\star$ is replaced with the matrix $\mathbf{\Phi}_\star \in \mathbb{R}^{3n_\star}$, which contains the basis functions for $n_\star$ test locations. Now the latent function values $\mathbf{f}_\star = [f_{\star,1},\ f_{\star,2},\ \ldots,\ f_{\star,n_\star}]^\top \in \mathbb{R}^{n_\star}$ can be predicted using the predictive equations (mean and variance) for the reduced-rank approximation from [43] as

$$\begin{aligned}\mathbb{E}[\mathbf{f}_\star] &\approx \mathbf{\Phi}_\star \left(\mathbf{\Phi}_{1:n}^\top\mathbf{\Phi}_{1:n} + \sigma_{\mathrm{y}}^2\mathbf{\Lambda}^{-1}\right)^{-1}\mathbf{\Phi}_{1:n}^\top\mathbf{Y}_{1:n},\\ \mathbb{V}[\mathbf{f}_\star] &\approx \sigma_{\mathrm{y}}^2\mathbf{\Phi}_\star\left(\mathbf{\Phi}_{1:n}^\top\mathbf{\Phi}_{1:n} + \sigma_{\mathrm{y}}^2\mathbf{\Lambda}^{-1}\right)^{-1}\mathbf{\Phi}_{1:n}^\top.\end{aligned} \tag{2-25}$$

Instead of inverting a $n \times n$ matrix, now only a $n_b \times n_b$ matrix needs to be inverted, speeding up the process and reducing computational requirements when $n_b < n$.

2-3-2 Reduced-rank hyperparameter training

In Section 2-2-3 the hyperparameter training for the full GPR frame-work has been discussed. The steps for the hyperparameter training for the reduced-rank approximation are similar. The approach of Solin *et al.* [43] is followed, and hence the matrix $\tilde{\mathbf{Q}} = \mathbf{\Phi}_{1:n}\mathbf{\Lambda}\mathbf{\Phi}_{1:n}^\top + \sigma_{\mathrm{y}}^2\mathcal{I}$ is defined. The terms in the objective function and its gradient function are expressed according to [43] respectively as

$$\tilde{\mathcal{L}}(\boldsymbol{\theta}) = \frac{1}{2}\log|\tilde{\mathbf{Q}}| + \frac{1}{2}\mathbf{y}^\top\tilde{\mathbf{Q}}^{-1}\mathbf{y} + \frac{n}{2}\log 2\pi, \tag{2-26}$$

and

$$\frac{\partial\tilde{\mathcal{L}}(\boldsymbol{\theta})}{\partial\theta_j} = \frac{1}{2}\frac{\partial\log|\tilde{\mathbf{Q}}|}{\partial\theta_j} + \frac{1}{2}\frac{\partial\mathbf{y}^\top\tilde{\mathbf{Q}}^{-1}\mathbf{y}}{\partial\theta_j}. \tag{2-27}$$

The full derivations are formulated by Solin and Särkkä [43]. Moreover, a change of variables in the form of

$$\theta_j^2 = \exp(s_j) \tag{2-28}$$

helps to ease the optimization.

2-4 Magnetic field mapping with a motion capture suit

Veen [38] used a MOCAP suit for magnetic field mapping and modeled the magnetic field as the gradient of a scalar potential using a reduced-rank method. In this research the same suit is used to conduct the experiments. The MOCAP suit enables accurate position estimation due to the high quality sensors and the software of the suit. Several body segments are equipped with sensors, i.e. an inertial measurement unit (IMU) and a magnetometer. Drift between the body segments is avoided by incorporation of biomechanical constraints. The settings of the MOCAP suit incorporate the information that the floor level of the experiment site is flat. The drift of the altitude of the suit is removed by contact detection with the ground [17]. The absolute position of the suit in the walking directions is subjected to drift, but this drift is continuously corrected by the MOCAP suit [17]. In this work it is assumed that the position estimations from the suit are sufficiently accurate to neglect the consequences of the drift, i.e. it is assumed that the body segments of the MOCAP suit are known. Magnetic field maps are regularly used for localization, e.g. in SLAM, where the location of the user on the map is updated. In these scenarios the absolute position is accurately determined and the influence of drift is restricted.

With multiple magnetometers available, it is possible to take multiple measurements at each time-step. An advantage of the MOCAP suit is that all magnetometer measurements are synchronized, i.e. collected at the same time-step. The reduced-rank method from Solin and Särkkä [43] is applied to the data from the MOCAP suit. The magnetometer locations and corresponding measurements are formulated as

- $\mathbf{x}_{i,k}^{\mathrm{n}} \in \mathbb{R}^3$, the 3D input location of magnetometer i at time-step k.
- $\mathbf{y}_{i,k}^{\mathrm{n}} \in \mathbb{R}^3$, the normalized 3D magnetic field strength of magnetometer i at time-step k.

The basis function matrices from Section 2-3-1, $\boldsymbol{\Phi}_{1:n}$ and $\boldsymbol{\Phi}_\star$, are extended. Contrary to the foregoing case, each time-step k now counts n_m measurements, instead of one. Consequently, the basis function matrices are constructed using blocks of $\boldsymbol{\Phi}_{k,m}$ with $k = 1,\ldots,n$ and $m = 1,\ldots n_m$. These matrices are used similar to previous section to approximate the kernels required for full GPR.

2-5 Evaluating performance

The reduced-rank GPR model gives the predictive mean $\mathbb{E}[f_{\star,i}]$ and the predictive variance $\mathbb{V}[f_{\star,i}]$ for $i = 1, \ldots, n_\star$ test points. In this research the root mean squared error (RMSE) and the mean standardized log loss (MSLL) are used to evaluate the quality of the estimates from the prediction method. These metrics, or variations thereof, are described by Rasmussen and Williams in [35]. The RMSE is used to examine the performance in terms of the difference between the predictions and the targets at the test locations. It is formulated as

$$\text{RMSE} = \sqrt{\frac{1}{n_\star} \sum_{i=1}^{n_\star} \| y_{\star,i} - \mathbb{E}\left[f_{\star,i}\right] \|_2^2}. \tag{2-29}$$

The MSLL includes information from the predictive variance. This metric is formulated as

$$\text{MSLL} = \frac{1}{n_\star} \sum_{i=1}^{n_\star} \left(\frac{1}{2} \log\left(2\pi\sigma_{\star,i}^2\right) + \frac{\left(y_{\star,i} - \mathbb{E}\left[f_{\star,i}\right]\right)^2}{2\sigma_{\star,i}^2} \right), \tag{2-30}$$

with $\sigma_{\star,i}^2 = \mathbb{V}[f_{\star,i}] + \sigma_{\mathrm{y}}^2$. For both the RMSE and MSLL holds that a lower value implies a better model fit.

Chapter 3

Analysis and experiments

The MOCAP suit is used to collect experimental data for modeling the ambient magnetic field using multiple magnetometers. The aim of the experiments is to understand how the measurement data from the MOCAP suit are used to obtain a high-quality magnetic field map for indoor localization. More specifically, the benefits and challenges of using multiple magnetometers from a motion capture suit to model the ambient magnetic field in indoor environments are researched. From the previous chapter, it is concluded that Gaussian processes are a useful tool for modeling the ambient magnetic field, also if multiple magnetometers are used to collect the magnetic field measurements. However, the GPR framework requires a single set of hyperparameters to model the magnetic field at all magnetometer locations. It is expected that optimal hyperparameters differ for the individual magnetometer measurements. It is expected that the optimal hyperparameters for measurements of magnetometers operating at similar altitudes are equal (or closely related). Under the assumption that the effect of the walls on the anomalies of the ambient magnetic field is limited, the relation between the magnetometer's altitude and the 'behavior' of spatial variations is expected to be seen. Magnetometer measurements near the ground are expected to show more and larger variations than the measurements from magnetometers at larger altitudes. If this expectation is supported during the experiments with the MOCAP suit, then the question arises how these data are used to make a magnetic field map.

Magnetic field mapping using a MOCAP suit is not common. Veen [38] used the MOCAP suit to model the magnetic field using reduced-rank GPR as the gradient of a scalar potential, but the focus of his work lies in SLAM. Veen concluded that magnetic field mapping with a combination of magnetometers of the MOCAP suit is a promising field for further research. The MOCAP suit was also used in [39] for magnetic field mapping, but only a single magnetometer was used.

In Section 3-1 the specific MOCAP suit for conducting the experiments is introduced. The output data of the MOCAP suit are inspected in Section 3-2. In this section it is researched how the spatial variations in the ambient magnetic field change in an indoor environment. The influence of the proximity of magnetic field disturbing sources on the magnetic field anomalies is also examined. The hypothesis that the spatial variations vary with altitude is confirmed, but the influence of the ferromagnetic materials in the walls is also observed. In Section 3-3, the optimal hyperparameters for the data of the seventeen magnetometers are determined separately. The GPR framework requires one set of hyperparameters to describe the measurement data of all magnetometers in the MOCAP suit. It is expected if the magnetic field characteristics differ at each magnetometer location, also the optimal hyperparameters describing its data differ per location. This may complicate finding a single set of hyperparameters that is suitable for describing data of a subset of magnetometers in Section 3-4. In this section the benefits and challenges of combining multiple magnetometers of the MOCAP suit to model the magnetic field of the indoor experiment site are determined. To this end, magnetometers operating at similar altitudes are collected in a subset. Moreover, the walking method is alternated, since this affects at what altitude certain magnetometers operate. The idea behind moving in different ways is to influence the number of magnetometers operating in a specific range of heights.

3-1 Experimental set-up

The magnetic field map is made using the data from the MOCAP suit. In this section the hardware for the experiments is introduced, and the calibration method is explained.

3-1-1 Introduction to the Xsens MVN Link motion capture suit

The MOCAP suit which is used in this research is the MVN Link suit from Xsens [17]. The suit is equipped with seventeen magnetometers, which return measurements of the magnetic field in three dimensions and have a sampling rate up to 240 Hz [44]. The measurements are normalized, hence in absence of anomalies in the magnetic field the magnetometer returns a measurement vector with a norm (magnitude) equal to 1. In this research, the deviations from the norm of the ambient magnetic field are captured in a map.

The software of the suit contains advanced methods to reduce positional drift [17]. The advantage of the suit is that it returns the locations of the body segments expressed in the navigation coordinate frame. In absence of additional hardware to determine the absolute location of the suit, it is assumed that the true magnetometer locations are returned by the MOCAP suit. The implication of this assumption is twofold. Firstly, the assumption implies that for the duration of the experiments, the drift in the magnetometer locations is sufficiently small to represent the true absolute position of the suit. Secondly, it implies that the true locations of the magnetometers are returned by the MOCAP suit. However, the Xsens MVN Link MOCAP suit merely returns the locations of 24 body segments (and not the 17 magnetometer locations). These locations do not coincide with the magnetometer positions. In this research it is assumed that the output of each magnetometer is measured at the nearest body segment location.

The magnetometer locations of the Xsens MVN Link MOCAP suit are the following: pelvis (P), neck (N), head (H), right shoulder (RS), right upper arm (RUA), right forearm (RFA), right hand (RH), left shoulder (LS), left upper arm (LUA), left forearm (LFA), left hand (LH), right upper leg (RUL), right lower leg (RLL), right foot (RF), left upper leg (LUL), left lower leg (LLL), left hand (LH).

3-1-2 Calibration

The magnetometers of the suit are calibrated in accordance with the magnetic field mapper manual [45]. They must be calibrated in a uniform magnetic field, without any anomalies. To this end, the calibration is performed outside. All seventeen magnetometers of the suit are rotated simultaneously by rotating the unequipped suit for a few minutes using both hands, whilst keeping the battery pack as far away from the sensors as practically possible. After calibration of the magnetometers the body segments of the suit are calibrated in accordance with the Xsens MVN Link user manual [44] and it is performed whilst wearing the suit. The user's body dimensions are specified to achieve an optimal calibration (see Appendix A).

3-2 Inspecting the magnetometer measurements

The individual contribution of each magnetometer of the Xsens MVN Link MOCAP suit to the model is researched in this section. Specifically, the change in characteristics of spatial variations in the ambient magnetic field of an indoor environment is regarded. The spatial variations are expected to be influenced by the proximity of magnetic field disturbing sources in the ground and in the walls.

The measurements from the magnetometers of the suit are visualized to investigate how the spatial variations in the ambient magnetic field change in the experiment site. The ferromagnetic materials in the walls and the floor introduce perturbations in the earth's magnetic field. The effects of proximity of magnetic field disturbing sources in these walls and floor to the magnetometers are expected to be seen in the magnetometer data (e.g. see [16]). Therefore, it is expected that the magnetic field shows more and larger anomalies near the ground and walls than at larger altitudes and further away from the walls. The data for the experiments are collected in a building of TU Delft in the Netherlands. The perturbations in the indoor magnetic field are assumed to be temporally stable.

3-2-1 Experiment description

To compare different experiments along the same trajectory and to compare different trajectories in the same room, a grid of 5 m $\times$ 5 m is marked on the floor using tape. Using this grid, a consistent step size of one meter is maintained. A zigzag trajectory is followed (visualized in Figure 3-2). During post-processing the pelvis location is initialized at $(x_1, x_2) = (1, 1)$ and the rotation is initialized such that the walking directions are along the x_1- and x_2-dimension. The pelvis magnetometer starts at the first marker of the grid. There are three walls in close proximity to the boundaries of the grid.

The MOCAP data is split in a train dataset and a test dataset. The magnetometers of the Xsens MVN Link have a sampling frequency up to 240 Hz [44]. The train dataset is downsampled to 1000 measurements per magnetometer. The magnetometer data is not downsampled based on decreasing the sampling frequency. Instead, the data from the pelvis sensor is used to obtain 1000 magnetometer locations which have a minimum distance from each other to obtain approximately equally spaced measurements. The time indices for these 1000 locations are used to collect the magnetometer locations and their corresponding output values of all seventeen magnetometers, resulting in the magnetometer location vector $\mathbf{X}_{1:n} \in \mathbb{R}^{3nn_m}$ and the measurement vector $\mathbf{Y}_{1:n} \in \mathbb{R}^{nn_m}$. Consequently, the measurements from the sixteen remaining magnetometers are not necessarily equally spaced. The test dataset is a different subset with the locations and measurements for the seventeen sensors at 400 time steps found using a similar approach with less space between the pelvis locations. There is no overlap between the time indices used for the train and the time indices used for the test data.

3-2-2 Ambient magnetic field deviation

Firstly, the measurement data is visualized without performing GPR. Since the interest lies in the spatial variations of the ambient magnetic field, the deviations in the magnetic field are shown. The deviations are obtained as follows: the mean of the train measurements from all seventeen magnetometers is computed and subsequently this mean is subtracted from the train measurements. The deviations in the magnetic field norm for each magnetometer are shown in Figure 3-1. The dots represent the magnetometer locations, and the colors the magnetic field norm deviation. This trajectory is denoted 'trajectory A1', where 'A' indicates the starting direction, and '1' the method of moving (in this case that is standard walking).

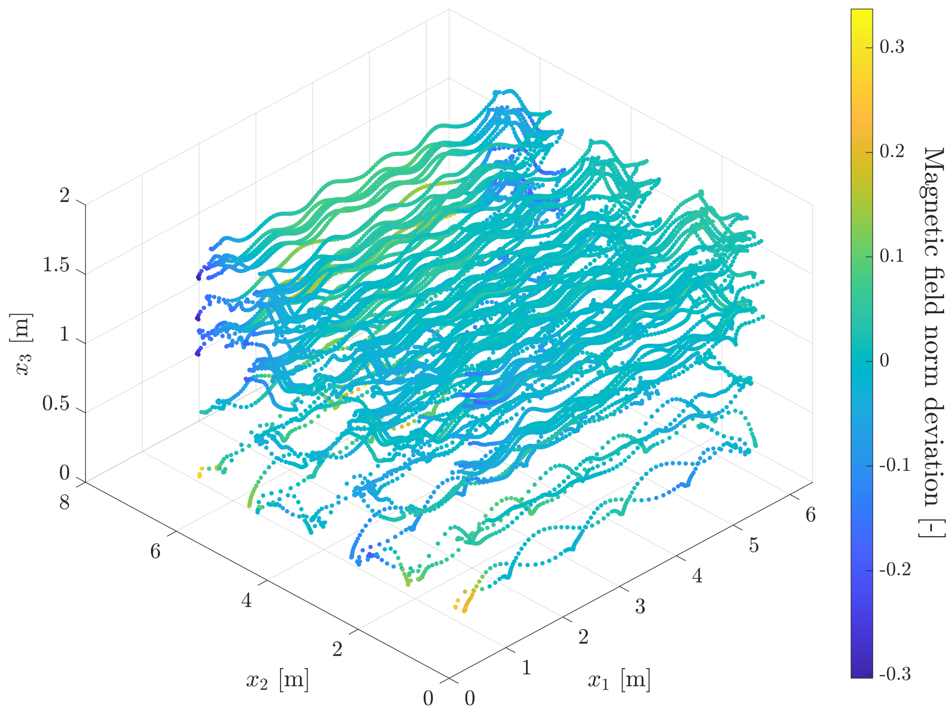

Figure 3-1: Train data whilst walking in the MOCAP suit. The color of the marker denotes the deviation of the magnetic field norm.

The minimum distance between the pelvis measurements is slightly larger than 35 mm. The measurements of the remaining magnetometers are chosen based on the time indices of the pelvis magnetometer. Thus they are not downsampled similar to the pelvis magnetometer measurements, which explains the observation that the measurements from the magnetometers on the legs and feet (and swinging arms) seem more dotted that others. Most magnetometers move approximately at constant speed, but the magnetometers on the legs and feet do not, because these alternate between high and low speed as a result of taking steps.

It is observed that the magnetic field contains more spatial variations near the ground than at larger heights, which is in line with the observation that the magnetic field of an indoor location varies with altitude [16]. However, also spatial variations at larger altitudes are observed at the boundaries of the measurements, which for instance is seen in Figure 3-1 relatively high above the floor in the plane orthogonal to the x_2-axis at $x_2 \approx 6.5$ m. These anomalies are likely caused by the ferromagnetic materials in (or near) the walls, e.g. radiators attached to the walls or reinforced concrete. Hence, besides the floor also the walls play an important role regarding the magnetic disturbance.

The observation that there are areas with more spatial variations in the magnetic field than others is investigated further. In Figure 3-2 data from the same experiment is shown. In the left plot the top-view for the left upper arm magnetometer locations is shown, whereas the right plot shows the locations for the right foot magnetometer, again with the color indicating the magnetic field norm deviation. The left upper arm magnetometer is selected because it is far away from the ground and it is attached to the side of the suit that is furthest away from the wall with the radiator. The measurements from this magnetometer hence show little fluctuation in the magnetic field norm deviation. The other magnetometer that is used is the one mounted on the right foot of the suit, which hence is close to the ground and also close to the wall with the radiator. This results in more fluctuations in the magnetic field norm measurements.

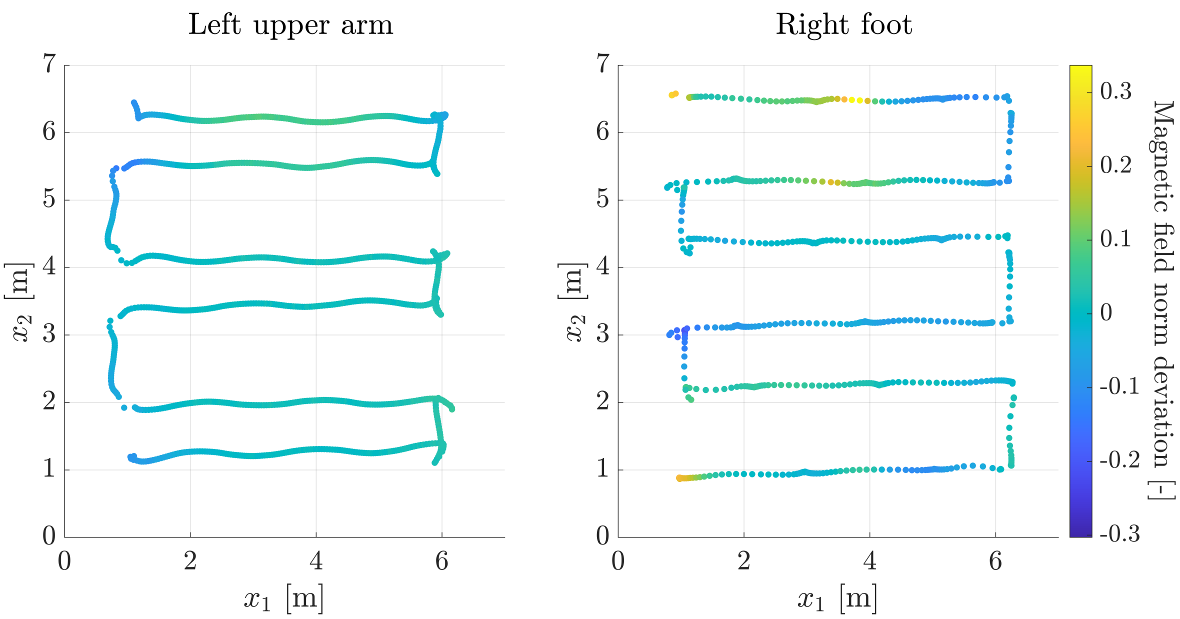

Figure 3-2: The post-processed train data from trajectory A whilst walking in the MOCAP suit. The left and right show respectively the data for the left upper arm and the right foot magnetometer. The color indicates the magnetic field norm deviation.

The measurements coming from the right foot magnetometer show a greater range and more spatial variations than the measurements from the left upper arm, leading to the conclusion that the hyperparameters that best fit the magnetometer measurements cannot be the same.

For the left upper arm data a large length-scale is expected. Informally put: relatively little spatial variations occur, hence a data point still contains some information on data points further away. For the right foot data, more spatial variations occur, and thus a smaller length-scale is preferred to model the rapidly changing deviations in the magnetic field. The downside is that a data point contains less information about data points further away, leading to rapidly growing prediction errors [35]. In the following section the magnetic field is modeled using the individual magnetometer measurements, where the variation in hyperparameters is examined.

3-3 Evaluation of reduced-rank GPR for a single magnetometer

In previous section it is verified that the magnetic field changes throughout the experiment site. More and larger anomalies are observed near the ground and near the walls than at larger altitudes and further away from the walls. The goal of this research is to investigate the benefits and challenges of using multiple magnetometers from the MOCAP suit for modeling the ambient magnetic field at an indoor environment. In this section, the hyperparameters are determined that best fit the data of each individual magnetometer. Subsequently, GPR is performed seventeen times, where each time the optimal hyperparameters for the data of one magnetometer are used to make predictions at all seventeen magnetometer locations. The aim of this section is to gain insight on which magnetometer locations contain useful information about other magnetometer locations. The findings of this section are used to improve the quality of the magnetic field map by composing magnetometer subsets based on similar hyperparameters in the last section of this chapter.

3-3-1 Determining hyperparameter values for the experimental data

Prior to finding the hyperparameters the reduced-rank approximation for GPR in Section 2-3 is initialized, i.e. a number of basis functions n_b is determined and the bounds of the domain of the map are set. The domain is based on the boundaries of the train data of all seventeen magnetometer locations. The domain is expanded by a margin of two length-scales on each side. Kok and Solin [28] use $n_b = 256$ basis functions for a domain that is similar in size (but different in shape). The amount of basis functions used in this work is further raised to $n_b = 400$, to be on the safe side.

When determining the amount of basis function and the domain for the reduced-rank framework, the hyperparameters to find the number of basis functions are based on literature. Preferably, the hyperparameters are optimized based on the magnetic field measurements from the experiments which were performed with the MOCAP suit. The hyperparameters of the reduced-rank GPR model are obtained by optimizing the NLML in Section 2-3-2. Once the optimal hyperparameter values are determined, the predictive equations in Eq. (2-25) are used to make the magnetic field map. However, the optimization of the NLML is difficult due to the highly nonlinear nature of the function. Therefore, a different approach is used in this section to find good hyperparameters for the magnetic field model. The combination of the length-scale and magnitude hyperparameter which yields the optimal NLML is determined based on a contour plot.

The NLML is evaluated for combinations of a set of length-scales $\ell_{\text{SE}} = \{0.2,\ 0.4,\ \ldots,\ 2\}$ and a set of magnitude hyperparameters $\sigma_{\text{SE}} = \{0.02,\ 0.04,\ \ldots,\ 0.2\}$. The noise hyperparameter is set to $\sigma_{\text{y}} = 0.02$. The same domain is used for each magnetometer, which is based on the outer locations of all seventeen magnetometers plus two times the length-scale on each side. The boundaries for the trajectory A1 (standard walking) are bounds $= [0.68\ 6.40\ 0.72\ 6.71\ 0.10\ 1.78]$ m. The optimal combination of length-scale and magnitude hyperparameter is found for each magnetometer. The resulting contour plots are shown in Figure 3-3.

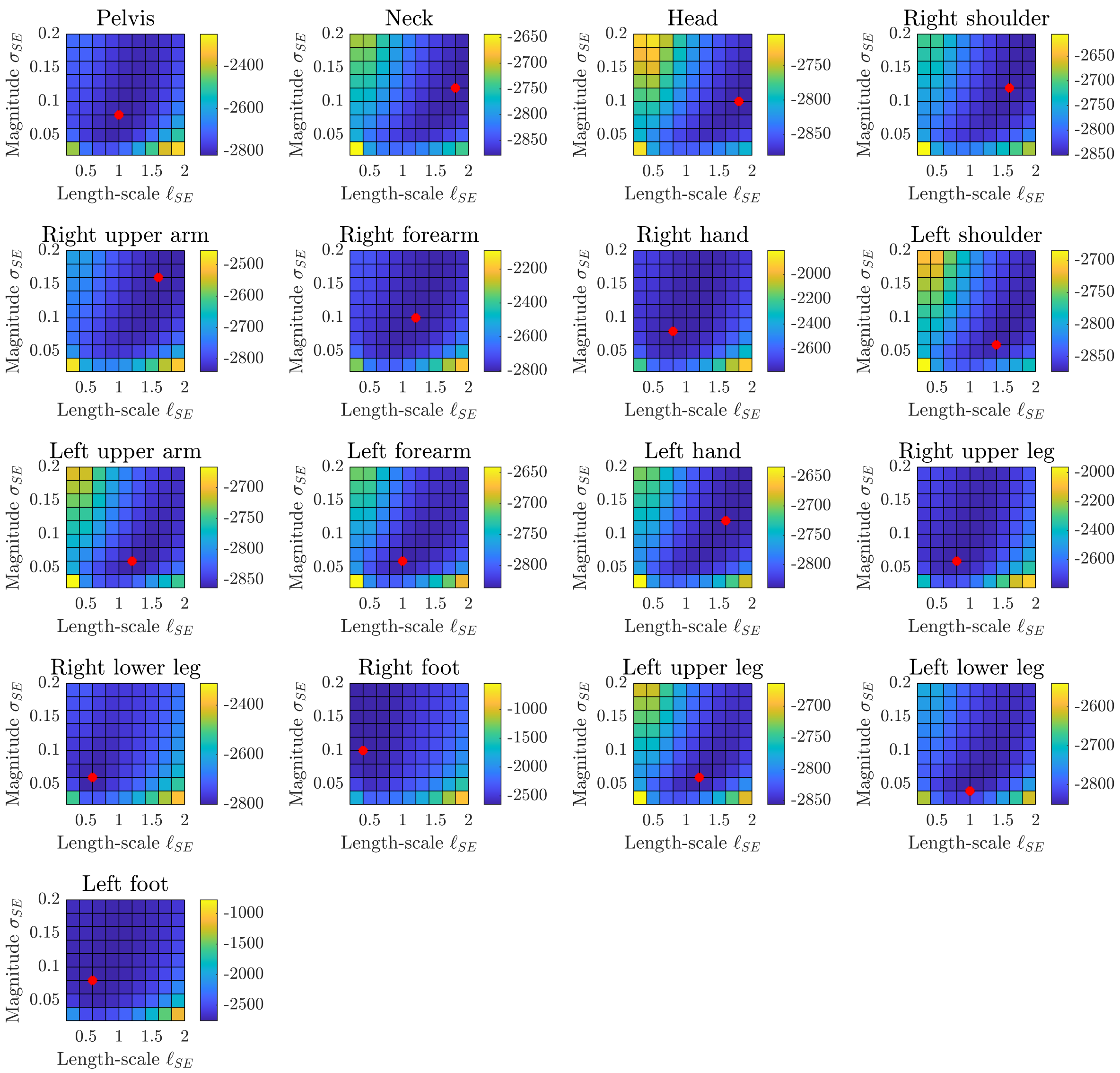

Figure 3-3: The NLML evaluated for different length-scale ℓ_{SE} [m] and magnitude hyperparameter σ_{SE} [-] pairs with the data from trajectory A1: standard walking. The optimal pair is indicated by a red dot.

It is expected to see the length-scale increase as the magnetometer's altitude increases. Further from the ground with its ferromagnetic materials, there are less anomalies in the ambient magnetic field. Magnetometers with the same height are therefore expected to have similar hyperparameters (specifically length-scales). Figure 3-3 confirms that the optimal hyperparameter values vary per magnetometer. Technically speaking, the red dots are (likely) not indicating the local optimal, since only a limited number of hyperparameter combinations are investigated. However, these values are considered to be optimal hyperparameter values in the remainder of this report. The interest lies in the influence of the (mean) height of the magnetometer on the observed magnetic field. Possibly, due to ferromagnetic structures in the walls, and radiators attached to the walls, a difference in optimal hyperparameters is also recognized in the left-hand-side and the right-hand-side of the suit, even if the magnetometers share the same height. The altitudes of the body segments (and thus the altitudes of the magnetometers under the assumption that these coincide) are accurately determined by the MOCAP suit. Therewith, the distance to the ferromagnetic materials in the ground is accurately determined. However, the distance between the walls and the MOCAP suit cannot be determined as accurately without additional hardware. To distinguish the anomalies in the magnetic field caused by the walls from those caused by the ground, the same pattern is walked but this time the trajectory starts along the x_2-direction (i.e. the trajectory in Figure 3-3 is mirrored along the diagonal of the x_1, x_2-plane). Consequently, the magnetometers on the left-hand-side of the suit are now for the major part close to the walls.

The hyperparameters for each single magnetometer are found similar to the aforementioned procedure. The amount of basis functions for the second experiment again is $n_b = 400$, and the domain is determined in the same way as described in Section 3-3-1. Figure B-1 in Appendix B shows the corresponding contour plots of each magnetometer. The results of both trajectories are summarized in Table 3-1.

In the table, the mean height of each magnetometer is shown. Because the measurements come from walking in a MOCAP suit the height of the magnetometers varies as a result of taking steps. However, these variations in height are small, which is confirmed by observing that the standard deviations of the magnetometer heights are mostly around 0.03 m.

From the table it becomes apparent that generally for higher magnetometer positions the minimum NLML is found at larger length-scales, whereas for lower magnetometer positions this minimum occurs for smaller length-scales. Moreover, it is confirmed that the optimal hyperparameters are different for left and right. However, the results are not always consistent. For instance, the optimal length-scale for the RUA magnetometer is for both trajectories larger than for the LUA magnetometer, and the difference is big (0.4 m for trajectory A and 0.8 m for trajectory B). The optimal length-scale for the neck (N) magnetometer, which has a mean height that is close to those of the shoulders and is positioned between them, lies not between the optimal length-scale values of both shoulders, looking at the results of trajectory A. Intuitively, the optimal length-scale value for the N magnetometer lies between those of the shoulders since the wall is on one side, and an empty room on the other, so at least a gradual change would be expected. This leaves the question to what extend these optimal hyperparameter values can be trusted.

	Trajectory A1				Trajectory B1			
Magnetometer position	Mean height [m]	Height std. dev. [m]	ℓ_{SE} [m]	σ_{SE} [-]	Mean height [m]	Height std. dev. [m]	ℓ_{SE} [m]	σ_{SE} [-]
H	1.725	0.032	1.8	0.10	1.738	0.034	1.4	0.08
RS	1.584	0.032	1.6	0.12	1.592	0.034	1.6	0.12
LS	1.583	0.032	1.4	0.06	1.594	0.034	1.4	0.12
RUA	1.557	0.034	1.6	0.16	1.573	0.035	1.6	0.10
LUA	1.553	0.034	1.2	0.06	1.584	0.037	0.8	0.06
N	1.504	0.031	1.8	0.12	1.513	0.033	1.4	0.08
RFA	1.272	0.033	1.2	0.10	1.291	0.033	1.4	0.12
LFA	1.268	0.033	1.0	0.06	1.305	0.033	0.8	0.08
LUL	1.091	0.031	1.2	0.06	1.102	0.034	1.0	0.08
RUL	1.089	0.030	0.8	0.06	1.096	0.033	1.4	0.08
P	1.089	0.030	1.0	0.08	1.098	0.033	1.0	0.08
RH	1.027	0.036	0.8	0.08	1.049	0.037	1.4	0.06
LH	1.022	0.036	1.6	0.12	1.065	0.038	0.8	0.08
LLL	0.576	0.025	1.0	0.04	0.593	0.018	0.6	0.06
RLL	0.575	0.025	0.6	0.06	0.574	0.028	1.0	0.06
LF	0.158	0.064	0.6	0.08	0.159	0.055	0.6	0.14
RF	0.150	0.059	0.4	0.10	0.161	0.062	0.4	0.08

Table 3-1: Mean magnetometer heights and standard deviation of magnetometers and optimal hyperparameters based on contour plots for both standard walking trajectories A1 and B1.

3-3-2 Predicting the entire field using the data from a single magnetometer

Considering the hyperparameters, particularly for the length-scale holds that at larger altitudes larger length-scales are expected. However, also differences in the optimal length-scales between the left hand side and the right hand side are observed, which possibly is explained by the proximity of the walls around the experiment site. A clear increase or decrease of the magnitude hyperparameter related to the magnetometer altitude is not obvious. Therefore, the focus in this section is on the length-scale. The aim is to determine which magnetometer data potentially could be combined to improve the quality of the magnetic field map. Specifically, the point at which the combination of magnetometer data does no longer yield an improvement in the quality of the magnetic field map is sought.

The optimal hyperparameter values of Table 3-1 are used to perform reduced-rank GPR for each single magnetometer for the standard walk data sets. To examine the quality of the predictions made using the reduced-rank GPR, the RMSE and MSLL (respectively Eq. (2-29) and Eq. (2-30)) are evaluated for all seventeen magnetometers. The train data of each magnetometer is used to make predictions on all seventeen magnetometer locations. The RMSE is evaluated between the test data from each magnetometer and the predictions on these locations. The same holds for the MSLL. The results of trajectory A1 and B1 are shown in Figure 3-4 and Figure 3-5 respectively. The axes are sorted on mean height of the magnetometers for trajectory A1.

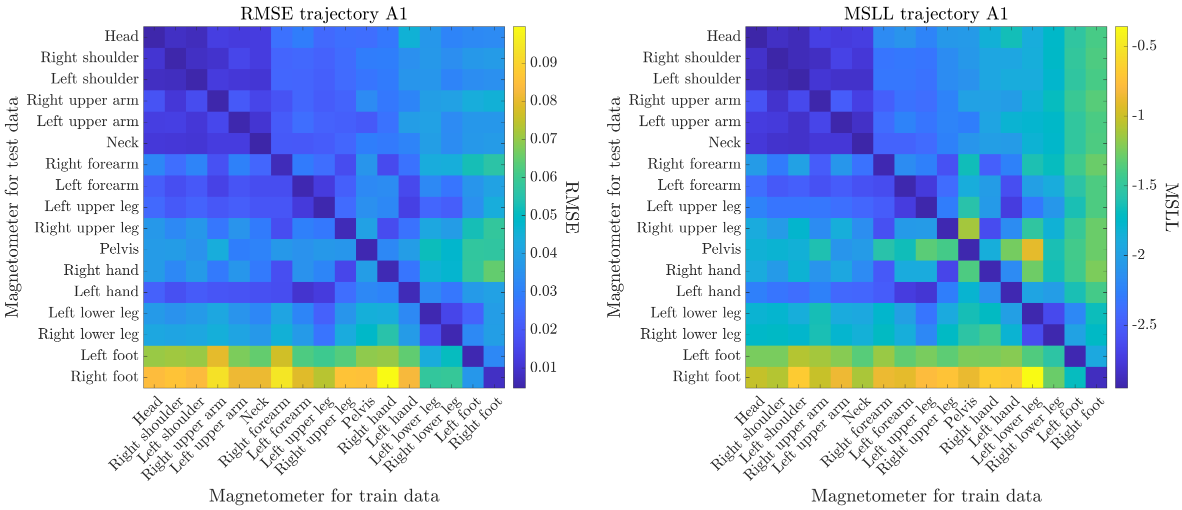

Figure 3-4: The performance metrics for the standard walking experiment for trajectory A1 where data from a single magnetometer is used to make predictions at all magnetometer locations.

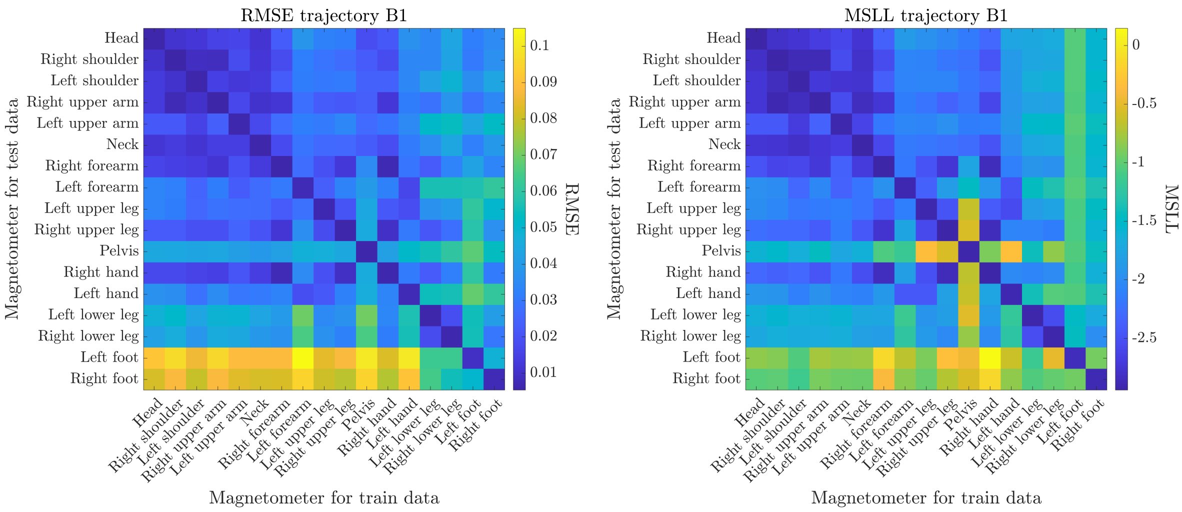

Figure 3-5: The performance metrics for the standard walking experiment for trajectory B1 where data from a single magnetometer is used to make predictions at all magnetometer locations.

The first observation regards the diagonals in each plot with low RMSE and MSLL values. When the train data of a magnetometer is used to make predictions on the test data of the same magnetometer, the errors between the real values and the predictions are low, and the certainty of the predictions is high. When the RMSE is low, indicating that the train data can be used to make accurate predictions on the magnetometer location under consideration, it is observed that the MSLL is also low. And vice versa if the RMSE is high, then the MSLL is also high. Hence, there is no need to make a trade-off between a low RMSE or a low MSLL.

A second observation regards the performance of the pelvis magnetometer. The metrics at its test locations when the train data from the pelvis magnetometer is used are comparable to the other cases when the train data of a magnetometer is used to make predictions at its own test locations. However, relatively high RMSE and MSLL values are seen when the pelvis magnetometer is used to make predictions on the other magnetometer locations, and neither the metrics for the predictions of the magnetic field on the pelvis location based on the data of other magnetometers are low. This poor performance is most likely explained by the presence of the battery pack of the suit near the pelvis. The effects of the materials of the battery pack are not corrected during calibration, because the battery pack was hanging below the suit to avoid that the other magnetometer calibrations would be disturbed by its presence. The distance between the pelvis magnetometer and the battery pack was significantly larger during calibration than during the experiments. This problem holds for each recording with the MOCAP suit, and therefore the magnetometer readings from the pelvis are disregarded in the remaining experiments.

Another observation regards the information the train data of one magnetometer provides about the magnetic field on the test locations of the remaining magnetometers, i.e. the cross-correlation between the magnetometers. Figures 3-4 and 3-5 show there are strong cross-correlations between the magnetometers with a mean height larger than 1.5 m (recall Table 3-1). Using the train data from either the H, RS, LS, RUA, LUA, or N magnetometer, the predictions on the test locations for these magnetometers are relatively good (the RMSE $<$ 0.02 in most cases). In trajectory A1, each of these six magnetometers can achieve predictions with a RMSE around 0.03 for the LFA, LUL, and LH magnetometer, the predictions for the RFA, RUL, and RH magnetometer are worse, with a RMSE around 0.04. The same observation is made in trajectory B1, but then left and right are interchanged. Note that the other way around, i.e. when the forearm, upper leg, or hand magnetometer is used for predicting the magnetic field at the H, RS, LS, RUA, LUA, or N magnetometer, the RMSE is not as low.

The cross-correlation between the forearm, upper leg, and hand of each side yields a RMSE around 0.03, but the information from one side seems not to contain much information about the other side. An explanation for this observation lies in the walls around the experiment site. For trajectory A1, where the walls are mostly on the right-hand-side of the suit the cross-correlation between the magnetometers is weaker compared to the left-handed side. The opposite holds for trajectory B1, where the walls are mostly on the left side: the predictions on the left-handed side suit show lower values for RMSE and MSLL than those of the right-handed side. This suggests that, regardless of the close range in magnetometer height ($\approx$ 1.00 m $-$ 1.20 m), the optimal hyperparameters still can vary significantly due to the walls.

The lowest four magnetometers (LLL, RLL, LF, RF) do not contain any information on the other magnetometer location. Contrary to the other magnetometers, with exception of the pelvis, predictions made with these four magnetometers often results a RMSE larger than 0.05. The length-scales that best fit the data of from these four magnetometers are significantly smaller than the other magnetometers, and the distances between the other magnetometers are quite large (the feet operate at a height around 0.16 m, the lower legs around 0.57 m and the hands follow at around 1.02 m). The lower legs contain information on each other's positions looking at the cross-correlations, but the information from the feet cannot be used to make accurate predictions on each other's location.

In conclusion, when the train data of a magnetometer is used for making predictions at the test locations of this same magnetometer, the RMSE is low (below 0.01) and the MSLL is also low (below -2.5). When the magnetic field at the test locations is modeled using the train data from a magnetometer at another location, the errors of the predictions vary. Generally, when the difference in height of the train and test locations increases, the predictions show larger values for the RMSE and the MSLL. However, it is shown that in some cases the height of the magnetometers for test and train data may be comparable, but nevertheless relatively high RMSE and MSLL values are observed. Possibly this is a result of the walls surrounding the experiment site which contain ferromagnetic materials which disturb the ambient magnetic field nearby, which is observed by the magnetometers near the wall, but not by the magnetometers on the other side of the suit.

3-3-3 Moving in different ways

The goal of the research is to explore the benefits and challenges of using a MOCAP suit for mapping the ambient magnetic field. The magnetometers of the MOCAP suit can move with respect to each other, by moving in different ways. This motivates to examine the influence of different walking methods. By moving differently from the 'standard' walking method, the magnetometers of the suit may operate at different altitudes and possibly the amount of magnetometers in a certain range of heights is alternated, compared to other walking methods. Specifically, the impact of different positions of the arms are researched, as well as a moving method where all magnetometers operate compactly and near the ground. The experiments of the 'standard' walking method are repeated. The following types of moving are discussed:

- Standard walking: walking with a normal posture where each step is 1 m.
- T-pose walking: walking with the arms stretched to left and right such that a T-shape is formed, again with steps of 1 m.
- Frog-like walking: each time both hands are placed on the 1 m markers, and in a hopping movement the feet are placed behind the hands. This way of moving is compared to the movement of a frog, but then without the jumping.
- Arms-high walking: walking with both arms stretched out upright, with steps of 1 m.

Like the standard walking method discussed in previous section, the three additional walking methods are selected such that a magnetometer operates at approximately the same altitude for the whole duration of the experiment. The same paths as the standard walking method are followed. Trajectories A1-A4 denote the trajectory shown in Figure 3-1 for respectively 'standard walking', 'T-pose walking', 'frog-like walking', and 'arms-high walking'. Trajectories B1-B4 idem, but then the starting direction is along the x_2-direction. Similar to the procedure before, the number of basis function is set to $n_b = 400$ and the domain is determined by adding twice the length-scale to the bounds of the domain. Thereafter the hyperparameters are determined, where the results are shown in Appendix B-1. The equivalent tables of Table 3-1 and the equivalent figures of Figure 3-4 and 3-5 are placed in Appendix B-2 and B-3. The results are summarized below.

Hyperparameters

The hyperparameters for each walking method are determined in the same fashion as described in Section 3-3-1. For some of the moving methods, the optimal hyperparameter values where on the border of the domain ($\ell_{\text{SE}} \in [0.2 - 2.0]$, $\sigma_{\text{SE}} \in [0.02, 0.2]$). If the hyperparameter value is on the minimum edge of the border, this value is assumed to be optimal. If the hyperparameter is on the maximum edge of the border, additional hyperparameter values are scrutinized. This is the case for the RUA, LFA, and LH magnetometer for trajectory B2 (T-pose walking), and the H and LUA magnetometer for trajectory A4 (arms-high walking). The contour plots for finding the optimal hyperparameters of these magnetometers are also shown in Appendix B.

T-pose walking

The results for the T-pose walking experiment are similar to those of the standard walking experiment. The RMSE values for the cross-correlations of the five highest magnetometers are below 0.02, and when the four magnetometers near the ground are used to make predictions on the other thirteen magnetometer locations with the RMSE values mostly are higher than 0.03. Only the arms have a different position during the experiments. Consequently, the main differences between standard walking and T-pose walking are observed for the forearm and hand magnetometer which are on the wall-side. Because these magnetometers are near the wall (the hand even touches the walls during the experiments), the magnetic field observed by these magnetometers is not representative for the magnetic field in the room. Considering trajectory B2, the length-scales found for the LFA and the LH magnetometer are very small (0.2 m) compared to the standard walking trajectory A1 (0.8 m). The impact of the wall is less visible for trajectory A2. For trajectory A2 the RMSE values for the LFA and the LH location lay around 0.03 - 0.04, but for trajectory B2 the RMSE exceeds 0.05.

Frog-like walking

It is expected that for the frog-like experiment, the cross-correlation between the magnetometers is high since the magnetometer configuration is compact. The magnetometers are moving compactly through the room. Since the magnetic field near the ground contains more anomalies, smaller length-scales are required to model the magnetic field. With all magnetometers close to one another, there are sufficient measurements taken to make an accurate magnetic field map. However, the results do not confirm this hypothesis. There seems to be little cross-correlation between the magnetometers near the ground. Again, the upper six magnetometers (H, RS, LS, RUA, LUA, and N) show strong cross-correlations where the RMSE is below 0.03, but little cross-correlation are observed between the other magnetometer locations, where the RMSE often exceeds 0.04.

Arms-high walking

The cross-correlations for the upper ten magnetometers in the arms-high moving method yield low RMSE values (for trajectory A4 below 0.03, but for trajectory B4 below 0.05). Within these ten magnetometers two groups of magnetometers are distinguished with cross-correlations which yield even lower RMSE values (below 0.01). The first group consist of the RH, LH, RFA, and LFA magnetometer, whereas the second group contains the H, RUA, LUA, RS, LS, and N magnetometer. The performance of the lower legs and the feet are similar to those in the standard walking and T-pose walking.

3-4 Interpolation to different heights

The benefits and challenges of combining multiple magnetometers of the MOCAP suit to create a 3D magnetic field map are researched in this section. The hypothesis that a combination of magnetometers will improve the quality of a magnetic field map is examined. The performance metrics (the RMSE and the MSLL) at the test locations of each magnetometer are evaluated to assess the quality of the map. The experiments of previous section confirm what Hanley *et al.* [16] also found, that a change in magnetic field characteristics over the height is observed. An increase in length-scales is observed as the altitude of the magnetometer increases. However, there are some exceptions where the length-scale at a larger altitude is smaller than those at lower altitudes and the walls seems also to play a role in disturbing the ambient magnetic field regardless of the height. On one hand, using more magnetometers implies more information about the ambient magnetic field is obtained, on the other hand the optimal hyperparameters of the individual magnetometers are further apart than when a subset of magnetometers is used, and in the Gaussian process regression framework the hyperparameters are assumed to be the same for all magnetometers. In this section, the effect of different magnetometer combinations is researched for each of the four moving methods.

3-4-1 Inspecting the hyperparameters of a subset of magnetometers

The four walking methods discussed in Section 3-3-3 are compared. For each walking method, four scenarios regarding the magnetometer combinations are considered to make predictions on the magnetometer locations:

- Individual: for each of the sixteen magnetometer test locations, predictions are solely based on its own train data.
- Combination 1: magnetometers are grouped based on small differences in height (0.30 m - 0.40 m). The magnetometer measurements of the group are combined to make predictions on the test locations of the magnetometers in this group.
- Combination 2: magnetometers are grouped based on large differences in height (approximately 0.75 m and for the frog-like moving method 0.50 m). The magnetometer measurements of the group are combined to make predictions on the test locations of the magnetometers in this group.
- All: all sixteen magnetometers are used for the train data to make predictions at the test points for each magnetometer.

The experiment is repeated for each walking method. The specific range of heights for 'Combination 1' and 'Combination 2', and which magnetometers fall in that range, depends on the walking method. The results are summarized in Table 3-2 and Table 3-3 for 'Combination 1' and 'Combination 2' respectively. Only one set of hyperparameters can be chosen in the GPR framework to describe the measurement data, hence the mean value of the optimal hyperparameter values of the data from the magnetometer subset is used for modeling. When the optimal hyperparameters within a subset of magnetometers are far apart, the mean hyperparameters may deviate significantly from the optimal hyperparameters of the GP best describing the data of the individual magnetometers in that subset. The minimum and maximum value of the length-scale and magnitude hyperparameter are included in the table to quickly check if the mean value lies far from the optimal hyperparameters withing the subset of magnetometers. This section focuses on finding the hyperparameters of the combinations of magnetometers. The resulting hyperparameter values are later used to compare the influence of each walking method on the magnetic field map quality and to compare the influence on the magnetic field map quality when the subset of magnetometers is alternated.

Looking at the optimal hyperparameters for each height range, the following is observed in Table 3-2. Firstly, it is noticed that for magnetometer combinations below 1.40 m, there is a strong resemblance between the optimal hyperparameters of trajectory A and trajectory B. In many cases the mean length-scale is the same for both paths, and the mean values of the magnitude hyperparameters are close. Above 1.40 m, the difference between the mean magnitude hyperparameters of both trajectories remains small, but an increase in difference of mean length-scales is observed. Trajectory A has a length-scale that is about 0.4 m larger than trajectory B, when looking at the range 1.70 m - 2.10 m. Comparing the standard, T-pose, and arms-high moving methods, it is observed that for all mean height ranges, except 1.40 m - 1.70 m, the optimal length-scales are close. Regarding the magnitude hyperparameters, the mean of the optimal values is comparable between these ranges, but larger differences than for the length-scales occur. The position of the arms is alternated between these three moving methods, which mostly influences the magnetometer positions (and therefore magnetometer combinations) in the range of 1.40 m - 1.70 m. Therefore, it is especially interesting to compare the results of this range for the reduced-rank GPR with the magnetometer combinations.

Although similarities are seen in the mean values of the hyperparameters per height range for the standard, T-pose, and arms-high walking method, a large difference in the optimal hyperparameters within a subset of magnetometers is regularly observed. The height differences are relatively small with steps 0.30 m or 0.40 m, yet for each height range there is a walking method where the maximum length-scale is at least twice as long as its minimum length-scale. This weakens the correlation between the length-scale and the magnetometer altitude, which poses the question whether sorting the magnetometers on height will indeed improve the quality of the magnetic field map.

Arguably, the frog-like walking method shows similar length-scales for the range 0.00 m - 0.40 m, but looking at the range 0.40 m - 0.70 m, the ideal hyperparameters are significantly different from the other three walking methods (frog-like walking gives here mean length-scales of 0.5 m and 0.6 m, whereas the mean length-scales for all other methods are at least 0.8 m). Contrary to the frog-like moving method, the other three moving methods do not have any magnetometers in the range 0.70 m - 1.00 m. The possibility to compare this walking method to the others is therefore limited, but interesting conclusions may be drawn in comparison of magnetometer combination 1 and magnetometer combination 2.

When the height range is increased to 0.75 m (and 0.50 m for the frog-like walking method), similar results as before are observed. From Table 3-3 it is apparent that below 1.50 m the mean hyperparameters are close to each other when comparing trajectory A with trajectory B, whereas above 1.50 m larger differences occur.

Magnetometers	Mean height range [m]	Traj.	ℓ_{SE} [m] mean	ℓ_{SE} [m] min - max	σ_{SE} [-] mean	σ_{SE} [-] min - max
Standard walking						
H	1.70 - 2.10	A	1.8		0.10	
		B	1.4		0.08	
RS, LS, RUA, LUA, N	1.40 - 1.70	A	1.5	1.2 - 1.8	0.10	0.06 - 0.12
		B	1.4	0.8 - 1.6	0.10	0.06 - 0.12
RFA, LFA, LUL, RUL, RH, LH	1.00 - 1.40	A	1.1	0.8 - 1.6	0.08	0.06 - 0.12
		B	1.1	0.8 - 1.4	0.07	0.06 - 0.12
LLL, RLL	0.40 - 0.70	A	0.8	0.6 - 1.0	0.05	0.04 - 0.06
		B	0.8	0.6 - 1.0	0.06	
LF, RF	0.00 - 0.40	A	0.5	0.4 - 0.6	0.09	0.08 - 0.10
		B	0.5	0.4 - 0.6	0.11	0.08 - 0.14
T-pose walking						
H	1.70 - 2.10	A	1.8		0.08	
		B	1.4		0.08	
RUA, LUA, RS, LS, RFA, LFA, N, RH, LH	1.40 - 1.70	A	1.1	0.4 - 1.6	0.07	0.04 - 0.12
		B	1.3	0.2 - 2.6	0.13	0.06 - 0.24
LUL, RUL	1.00 - 1.40	A	1.1	0.8 - 1.4	0.06	
		B	1.1	1.0 - 1.4	0.06	
LLL, RLL	0.40 - 0.70	A	0.8		0.05	0.04 - 0.06
		B	1.0	0.6 - 1.4	0.06	
LF, RF	0.00 - 0.40	A	0.5	0.4 - 0.6	0.09	0.08 - 0.10
		B	0.3	0.2 - 0.4	0.06	0.02 - 0.10
Frog-like walking						
H, RS, LS, RUA, LUA, N	0.70 - 1.00	A	1.0	0.6 - 1.2	0.05	0.04 - 0.06
		B	1.0	0.6 - 1.2	0.07	0.04 - 0.10
LUL, RUL, RFA, LFA, LLL RLL	0.40 - 0.70	A	0.6	0.4 - 1.0	0.08	0.04 - 0.12
		B	0.5	0.2 - 1.0	0.07	0.04 - 0.10
RH, LH, LF, RF	0.00 - 0.40	A	0.4		0.07	0.06 - 0.08
		B	0.4		0.08	0.06 - 0.12
Arms-high walking						
RH, LH, RFA, LFA, H	1.70 - 2.10	A	1.8	1.2 - 3.0	0.08	0.04 - 0.18
		B	1.3	1.0 - 1.6	0.06	0.04 - 0.10
RUA, LUA, RS, LS, N	1.40 - 1.70	A	1.8	1.4 - 2.8	0.08	0.06 - 0.14
		B	1.4	0.8 - 1.8	0.10	0.06 - 0.12
LUL, RUL	1.00 - 1.40	A	1.0	0.8 - 1.2	0.06	
		B	1.2	1.0 - 1.4	0.07	0.06 - 0.08
LLL, RLL	0.40 - 0.70	A	0.8	0.6 - 1.0	0.05	0.04 - 0.06
		B	0.9	0.6 - 1.2	0.06	
LF, RF	0.00 - 0.40	A	0.5	0.4 - 0.6	0.09	0.08 - 0.10
		B	0.3	0.2 - 0.4	0.11	0.08 - 0.14

Table 3-2: Combination 1: magnetometer in a range of 0.30 m or 0.40 m are combined. The mean ℓ_{SE} and σ_{SE} are used for reduced-rank GPR. The minimum and maximum hyperparameters are shown to give an indication of the range of optimal hyperparameter values per height. Absent 'min - max' values indicate all hyperparameter values within that group are equal.

Magnetometers	Mean height range [m]	Traj.	ℓ_{SE} [m] mean	ℓ_{SE} [m] min - max	σ_{SE} [-] mean	σ_{SE} [-] min - max
Standard walking						
H, RS, LS, RUA, LUA, N	> 1.50	A	1.6	1.2 - 1.8	0.10	0.06 - 0.16
		B	1.4	0.8 - 1.6	0.09	0.06 - 0.12
RFA, LFA, LUL, RUL, RH, LH	0.75 - 1.50	A	1.1	0.8 - 1.6	0.08	0.06 - 0.12
		B	1.1	0.8 - 1.4	0.07	0.06 - 0.12
LLL, RLL, LF, RF	< 0.75	A	0.7	0.4 - 1.0	0.07	0.04 - 0.10
		B	0.7	0.4 - 1.0	0.09	0.06 - 0.14
T-pose walking						
H, RUA, LUA, RS, LS, RFA, LFA, N	> 1.50	A	1.4	0.4 - 1.8	0.07	0.04 - 0.12
		B	1.7	0.2 - 2.6	0.11	0.06 - 0.20
RH, LH, LUL, RUL	0.75 - 1.50	A	0.9	0.4 - 1.4	0.07	
		B	0.9	0.2 - 1.6	0.12	0.06 - 0.24
LLL, RLL, LF, RF	< 0.75	A	0.7	0.4 - 0.8	0.07	0.04 - 0.10
		B	0.7	0.2 - 1.4	0.06	0.02 - 0.10
Frog-like walking						
H, RS, LS, RUA, LUA, N, LUL, RUL	> 0.50	A	0.9	0.4 - 1.2	0.06	0.04 - 0.08
		B	0.9	0.2 - 1.2	0.07	0.04 - 0.10
RFA, LFA, LLL, RLL, RH, LH, LF, RF	< 0.50	A	0.5	0.4 - 0.8	0.08	0.06 - 0.12
		B	0.4	0.4 - 0.6	0.07	0.06 - 0.12
Arms-high walking						
RH - N*	> 1.50	A	1.8	1.2 - 3.0	0.08	0.04 - 0.18
		B	1.3	0.8 - 1.6	0.08	0.04 - 0.16
LUL, RUL	0.75 - 1.50	A	1.0	0.8 - 1.2	0.06	
		B	1.2	1.0 - 1.4	0.07	0.06 - 0.08
LLL, RLL, LF, RF	< 0.75	A	0.7	0.4 - 1.0	0.07	0.04 - 0.10
		B	0.6	0.2 - 1.2	0.09	0.06 - 0.14

* RH, LH, RFA, LFA, H, RUA, LUA, RS, LS, N

Table 3-3: Combination 2: magnetometer in a range of 0.75 m or 0.50 m are combined. The mean length-scale and magnitude hyperparameter are used for reduced-rank GPR. The minimum and maximum hyperparameters are shown to give a brief indication of the range of optimal hyperparameter values per height. When a 'min - max' value is absent, this indicates that all hyperparameter values within that group of magnetometers is equal.

3-4-2 Results for the combinations of magnetometers

Reduced-rank GPR is used to make predictions for the four different subsets ('Individual', 'Combination 1', 'Combination 2', and 'All'). The train data from each magnetometer subset are used to make predictions at the test locations of the magnetometers in the same subset. It is expected that using multiple magnetometers with a small range in mean height reduces the RMSE and the MSLL for the test locations within that subset. A correlation between magnetometer height and optimal hyperparameters is expected. When the height range is small, measurements with shared underlying characteristics are fused, improving the performance in terms of RMSE and MSLL compared to the individual magnetometer subsets. However, it is expected that fusing measurements from a broader range of magnetometer altitudes does not necessarily improve the predictions at the test locations of the magnetometers within the subset, because then the difference in optimal hyperparameters may be too big (and thus the mean of the optimal values for each single magnetometer does not represent the hyperparameters of the subset). The results for the RMSE are shown below. The MSLL results are shown in Appendix B-4.

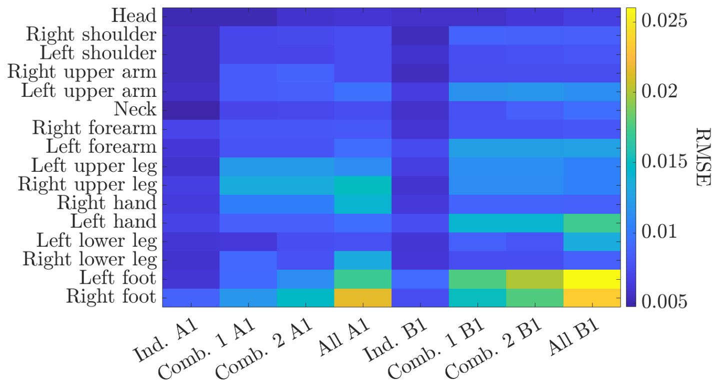

Figure 3-6: Comparison of the RMSE of the different magnetometer combinations for the standard moving method along trajectory A and B.

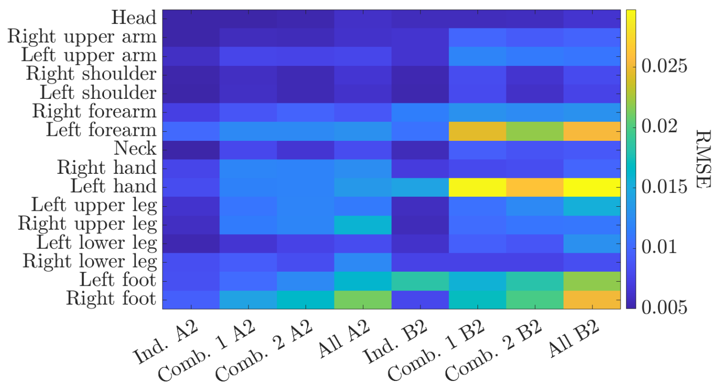

Figure 3-7: Comparison of the RMSE of the different magnetometer combinations for the T-pose moving method along trajectory A and B.

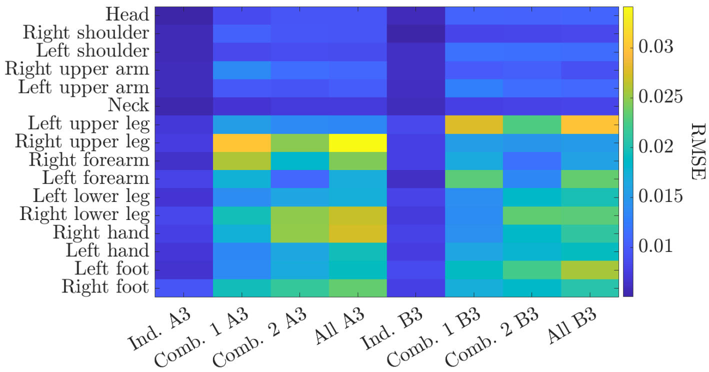

Figure 3-8: Comparison of the RMSE of the different magnetometer combinations for the frog-like moving method along trajectory A and B.

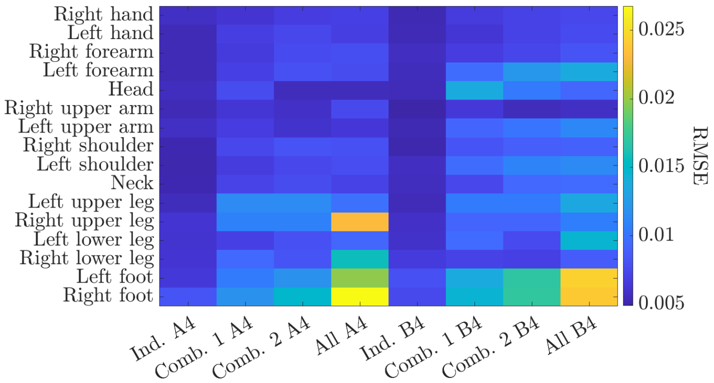

Figure 3-9: Comparison of the RMSE of the different magnetometer combinations for the arms-high moving method along trajectory A and B.

Recall the aim of this section is to investigate the benefits and challenges of combining multiple magnetometers of the motion capture suit to model the magnetic field. Now all ingredients are available to see what these benefits and challenges of the suit are. The results are categorized in three observations. Firstly, the impact of creating the magnetometer subsets is discussed, then observations related to the altitude of the magnetometers are made, and lastly the walking methods are compared to one another. Figure 3-6 to Figure 3-9 are obtained by evaluating the RMSE values as follows: a subset of magnetometers is used to make predictions at the test locations of the magnetometers in this subset. Using these predictions, the RMSE and the MSLL values are computed. The MSLL results are shown in Appendix B-4.

Comparing the influence of the magnetometer subsets the following is observed. It was expected that combining the data of a subset of magnetometers operating at similar altitudes would improve the magnetic field map, resulting in lower RMSE (and MSLL) values than when an individual magnetometer was used to make predictions on its on test locations, or when all seventeen magnetometers were combined to make the predictions. The subset yields lower RMSE and MSLL values than the case where the data of all seventeen magnetometers are used. However, this hypothesis is not supported when comparing to the case where the magnetometer measurements were used individually for of any of the walking methods. Using the train data of a single magnetometer to make predictions on the test locations of the same magnetometer yields better results than when the data of this single magnetometer is complemented with data from neighboring magnetometers. An increase in the RMSE and MSLL is observed as the amount of magnetometers in a subset increase. For the subsets at larger altitudes it seems that only for the T-pose walking method ‘Combination 2’ (with the larger height ranges) performs better than ‘Combination 1’ (with the smaller height ranges), as well as maybe the arms-high method, although this is not clear. For some individual magnetometers the RMSE) or MSLL) decreases, but that is at the cost of an increase in the RMSE (or MSLL) of the test locations from other magnetometers in the subset. It seems that the more magnetometer measurements are included in a subset, the more the map quality deteriorates, i.e. the RMSE and the MSLL at the test locations increase. Even if the magnetometers operate in a close range of mean height (which is the case for ‘Combination 1’) the RMSE increases.

Taking a subset of magnetometers rather than an individual one to make predictions on the test locations of the magnetometer in the subset leads in the majority of cases to an increase in the RMSE and the MSLL at the test locations of the magnetometers in the subset. The optimal hyperparameter values are regularly far apart, even when the data of magnetometers operating on the same height are combined. A possible explanation is found in the influence of the walls on the magnetic field. However, the negative effects of the walls are expected not to be the only reason why the RMSE and the MSLL increase when combining magnetometer data (with similar mean heights) in one subset. It is expected that the optimal hyperparameters for each magnetometer (found in Section 3-3-1) are not always representative for the magnetic field at the height of that magnetometer. For instance, based on Table 3-1 it was deducted that for the head and neck magnetometer the optimal hyperparameters varied 0.4 m, although the distance from the walls is similar for these magnetometers in the center of the suit. Also, for each walking method the difference in optimal hyperparameters for each magnetometer in the subset of the range 0.00 m to 0.40 m is small (max 0.2 m); there is little difference between left and right, thus the walls do not significantly influence the optimal hyperparameters. However, the subset that combines the magnetometers of this range still cannot reduce the RMSE and MSLL compared to those of the individual predictions at the test locations looking at Figure 3-6.

It looks as if the RMSE and MSLL at the test locations of the magnetometers close to the ground are larger than those of the magnetometers at larger altitudes. It was expected that this is due to the fact that there are less magnetometers operating close to the ground than at larger altitudes. Besides, steps of one meter are taken, whereas the optimal length-scales for modeling the magnetic field based on the measurements of the magnetometers on the feet were found to be around half a meter. Consequently, the magnetometer on one foot may be too far apart to contain information which can be used to improve the predictions about the magnetic field on the location of the other foot. However, also this hypothesis seems violated. In the frog-like walking method, there are more magnetometers near the ground than the other walking methods. Moreover, a smaller height range is considered when a subset of magnetometers is created. Nevertheless, the frog-like walking method shows the largest RMSE and MSLL values of all walking methods, especially at locations close to the ground.

Comparing the walking methods to one another, similarities are observed. The RMSE of the magnetometers at larger altitudes are lower than those of the magnetometers near the ground, especially compared to the feet. The RMSE values of the frog-like walking method are higher than the other moving methods. In the other movement methods only the position of the arms are changed. The effect of changing the position of the arms is hardly recognized, except for the 'T-pose' walking, where it is expected that the high RMSE values of the LFA and LH magnetometer are caused by the ferromagnetic materials in the walls.

In some cases the optimal hyperparameters were not found in the set of candidate hyperparameter pairs within $\ell_{\mathrm{SE}} \in [0.2, 2.0]$ and $\sigma_{\mathrm{SE}} \in [0.02, 0.2]$. The optimal length-scale for the LUA and LH magnetometer data for trajectory B2 (T-pose walking) were significantly smaller (0.2 m) than the other magnetometers operating on those heights. This is likely explained by the effect of the walls on the magnetic field where these magnetometers operate. The mean values of the length-scales of the subsets in which these magnetometers are included are much larger than this 0.2 m (in 'Combination 1' the mean length-scale is 1.3 m, and in 'Combination 2' it is 1.7 m for the subset in which the LFA is included and 0.9 m for the subset in which the LH is included). It was already seen that the predictions made using the measurements of these two magnetometers resulted in relatively large RMSE and MSLL values. In this section it becomes apparent again that the magnetic field for these magnetometers is too deviant compared to the magnetic field observed by the other magnetometers in the subset to model the magnetic field at the test locations of the magnetometers in the subset by using the same hyperparameters. The RMSE and the MSLL for these two magnetometers are large when the large length-scales of the subsets are used to model the magnetic field at their test locations.

Chapter 4

Discussion

The impact on the quality of a magnetic field map for indoor localization made using Gaussian processes with measurements from a MOCAP suit is researched in this report. The earth's magnetic field is perturbed in indoor environments due to the proximity of ferromagnetic structures in the floor and in the walls. It is confirmed that the length-scale of the reduced-rank GP for magnetometer measurements near the ground is smaller compared to the length-scales for magnetometer measurements operating at larger altitudes. However, the influence of the walls around the experiment site is also clearly visible in the magnetometer data: near the walls more spatial variations are observed than further away from the walls. The anomalies are temporally stable and provide valuable information for indoor localization. Several strategies in literature aim to improve the quality of a magnetic field map to reduce errors in position estimation, e.g. in the SLAM framework. Some of these methods combine the measurement data of multiple magnetometers, where the relative distances between the magnetometers and the global position of the assembly of magnetometers are known, to make a magnetic field map using GPR. The MOCAP suit can also be viewed as an assembly of magnetometers of which the position in the navigation frame is known, as well as the relative distances between the magnetometers. Because of contact detection with the floor, specifically the altitude of the magnetometers is accurately determined. It was expected that this feature of the MOCAP suit would play a central role in improving the quality of the magnetic field map.

Many authors have shown that GP's are a suitable tool for modeling the ambient magnetic field at indoor environments, and that the reduced-rank approximation can be used to reduce the computational complexity of GPR. The hyperparameters that best described the experimental data of the individual magnetometers from the MOCAP suit showed a correlation with the altitude. This observation is in line with the observation of Hanley *et al.* [16] that the spatial variations of the magnetic field in an indoor environment vary with altitude. However, the hypothesis that the correlation between the optimal hyperparameters of the GP and the magnetometer altitude could be exploited to improve the quality of a magnetic field map by combining data from different magnetometers of the MOCAP suit was not supported. Surprisingly, complementing the measurements from a single magnetometer with the measurements of its neighboring magnetometers did not lead to an improvement of the magnetic field predictions in terms of RMSE and MSLL at the test locations of a magnetometer compared to the case where only the data from a single magnetometer were used. The optimal length-scale of the GP for the data of an individual magnetometer increases with the magnetometer's altitude. The observation that combining the measurements of all seventeen magnetometers lacks an improvement in the performance metrics compared to the single magnetometer case is possibly explained by the fact that a compromise in the hyperparameters must be made. The optimal hyperparameters for the magnetometers at the largest altitude are distinct from the optimal hyperparameters describing the magnetic field near the ground. However, under this reasoning complementing measurements from magnetometers operating in a close range of heights is expected to improve the magnetic field map quality, i.e. it is expected to find lower RMSE and MSLL values at the test locations where the training data came from a subset of magnetometers which share approximately the same altitude than at the same test locations where the training data came from a single magnetometer. Unexpectedly, this hypothesis is not supported based on the conducted experiments. In a Gaussian process complementing the data that can be described with a certain set of hyperparameters with more data that can be described with the same set of hyperparameters should improve the resulting model. Hence, another explanation for this unexpected deterioration in performance metrics when combining magnetometer data is sought. Possible explanations are discussed below.

Firstly, the consistency between the magnetometers may be erroneous. It has not been verified if the magnetometers return identical outputs when placed in an identical position, but it is speculated that this may not be true. The measurements from the magnetometer on the pelvis showed deviant behavior, even after calibration, which possibly is explained by the proximity of the battery pack of the suit. The magnetometers have been calibrated according to the MVN Link user's manual [44]. However, the typical application for the Xsens MVN Link MOCAP suit is human motion tracking [17]. The magnetic field mapping method may be more sensitive to errors in the calibration of the magnetometers compared to motion capture. If it is true that the magnetometer data lack consistency, then this could be solved by complementing the post-processing of the MOCAP suit data with an additional calibration step. However, the magnetometers must all have measured the magnetic field at the same location, which was not the case in this research.

Secondly, the magnetometers of the MOCAP suit are subjected to positional errors, whose effects may show when combining magnetometer data. The Xsens MVN Link MOCAP suit returns the locations of 24 body segments expressed in the navigation coordinate frame, and the measurements of 17 magnetometers. The positions of the magnetometers cannot be retrieved. In absence of additional hardware to determine the true locations of the magnetometers, it is assumed that the measurements are collected at the nearest body segment location. In reality these locations do not coincide, and it is expected that the magnetic field map mostly is affected by the error in the altitude of the magnetometers (compared to the walking directions), because the magnetic field characteristics vary with altitude. It is expected that the influence of the altitude error on the quality of the magnetic field map decreases as the altitudes of the magnetometers increase, because far from the floor the magnetic field is less perturbed than close to the floor, i.e. at larger altitudes the magnetic field is more uniform than near the ground. However, this expectation cannot be verified without knowing the true magnetometer locations.

The third possible explanation for the deterioration of performance metrics when combining magnetometer data regards the influence of the walls on the ambient magnetic field. In the MOCAP suit settings it is specified that the ground surface is flat. This information is exploited to reduce the suit's, and therewith the magnetometers', positional drift in height. Consequently, the distance from the magnetometers to the ground with its ferromagnetic materials is accurately determined during the full experiment. The distance between the magnetometers and the walls not accurately known. Three walls surrounded the experiment site at a distance of approximately a meter, but the exact distance between the magnetometers and the walls in unknown. A difference in the optimal length-scales between the left hand side and right hand side was observed. It is expected that this difference is a result of the proximity of the walls around the experiment site. In absence of a possibility to retrieve the true distances between the walls and the magnetometers, two similar trajectories have been followed to distinguish the effects of the walls. In the first trajectory, the right hand side of the suit is mostly close to the walls, in the second trajectory, the left hand side of the suit is mostly close to the walls. The second trajectory is obtained by mirroring the path of the first trajectory along the diagonal. However, it would have been preferable to walk the identical trajectory in the opposite direction, because then the left hand side, right hand side, and center magnetometers of the first trajectory respectively traverse almost the identical path as the right hand side, left hand side and center magnetometers of the second trajectory. This allows for comparison between the optimal hyperparameters of the data of the individual magnetometers. If the optimal hyperparameters still differ in this proposed experiment set-up, conclusions can be drawn about the magnetometer calibration. Now the maps should look similar, but differences cannot be used to make statements about the magnetometer calibration because different parts of the indoor environment are visited while following the two trajectories. However, the first two reason as to why the deterioration of the performance metrics occurs are deemed more likely, since the measurements from Figure 3-1 show limited spatial variations caused by the walls.

Regarding the different movement methods, the following two observations are highlighted. One concerns the magnetometer subsets, the other the similarities between the movement methods.

When creating magnetometer subsets, it was observed that the magnetometer data from the subsets far from the ground yielded lower RMSE values and lower MSLL values than when the subsets of magnetometers near the ground were used. Two possible explanations are presented.

Firstly, the anomalies near the ground result in optimal length-scales around 0.2 m - 0.6 m (looking at the optimal length-scales of the feet), whereas the optimal length-scales for measurement data at larger altitudes are significantly larger. It is expected that the following observation explains why the RMSE values and MSLL values were larger near the ground. Steps of 1 m were taken, which is a large distance with respect to the length-scales for the data of the magnetometers near the ground. The magnetometers on the feet are frequently further than a length-scale apart. When this happens, the measurements from the magnetometer on one foot cannot be used to improve the predictions at the test locations of the magnetometer on the other foot. Moreover, the magnetometer measurements are downsampled based on the movement of the pelvis magnetometer. Consequently, the measurements of the magnetometers on the feet are dense when the feet stands still, but are spread out when moving (and thus when passing the other foot). Possibly, downsampling similarly to the pelvis magnetometer would have been preferred, since it is expected that this yields a better representation of the magnetic field near the ground. In that scenario the magnetometer measurements are no longer taken at identical time-indices, which is no problem for making a magnetic field map offline, but may cause complications when extending the approach to online mapping.

The second explanation regards the altitude error (as a consequence of the assumption that the magnetometer measurements come from the body segment locations). At larger altitudes the difference in height between magnetometers is smaller than near the ground. The optimal length-scales at larger altitudes are larger because the magnetic field contains less spatial variations and is more uniform. It is expected that the altitude error has therefore less influence on the magnetic field predictions at larger altitudes: if the magnetometer is wrongly positioned 20 cm higher or lower than its original location, the magnetic field may still look very similar. It is expected that the altitude error is more of a problem for magnetometers near the ground where many spatial variations are observed.

These two observations possibly explain the observation that the subsets at larger altitudes show lower RMSE and MSLL values than when the subsets of magnetometers near the ground were used to evaluate these metrics.

The second observation regarding the movement methods is the following. Changing the position of the arms for the walking methods appeared not to affect the estimates of the magnetic field significantly, except when the arms during the ‘T-pose’ walking method were touching the walls. The frog-like walking method showed larger RMSE and MSLL values than the other walking methods. It is not expected that the Xsens MVN Link MOCAP suit cannot model these movements sufficiently well, because the suit can even track movement while the user is crawling [17]. Possibly, when earlier issues related to the observation that the measurements of the magnetometers are not fully consistent are solved, other observations are made when conducting the same experiments.

Chapter 5

Conclusion and recommendations

In this research it is examined how the measurements from MOCAP suit improve the quality of the magnetic field map for an indoor location. Specifically, it is researched if a subset of the magnetometers provides better estimations of the magnetic field than when all magnetometers are used individually. The research question posed in the introduction is formulated as:

What are the benefits and challenges of using multiple magnetometers from a motion capture suit to model the ambient magnetic field in indoor environments?

The Xsens MVN Link MOCAP suit has been used to model the ambient magnetic field of an indoor environment. In Chapter 2 it was researched how multiple magnetometers of the motion capture suit could be combined to model the ambient magnetic field in indoor environments. Reduced-rank Gaussian process regression turned out to be a suitable tool for modeling the magnetic field due to its flexibility and the uncertainty information it provides, and its ability to cope with large datasets. The strength of the MOCAP suit is that the suit returns accurate locations of body segments, specifically when it comes to their altitude.

In Chapter 3 the change in spatial variations in the ambient magnetic field of an indoor environment was investigated. The influence of the proximity of magnetic field disturbing sources on the anomalies of the magnetic field was inspected. The ambient magnetic field at the experiment site showed more and larger anomalies in close proximity to the ground and walls than when the ground and walls were at larger distances. In accordance with literature, a relation between magnetic field characteristics and altitude was observed. Consequently, the hyperparameters of the Gaussian process that best fit the magnetometer measurements vary per magnetometer.

Moreover in Chapter 3 the benefits and challenges of combining multiple magnetometers of the MOCAP suit to create a 3D magnetic field map of an indoor environment were researched. In absence of the true magnetometer positions, it is assumed that each magnetometer is located at the nearest body segment. These body segments are accurately determined by the Xsens MVN Link MOCAP suit, especially regarding the altitudes. However, the data of each magnetometer is best described by different hyperparameters since the magnetometers operate at different altitudes and thus observe different magnetic field behavior. In the GP framework a single set of hyperparameters must be selected, which leads to the expectation that a subset of magnetometers improves the map quality (in terms of RMSE and MSLL) compared to used all magnetometers combined or using all magnetometers individually. This hypothesis is not validated during the experiments. Generally, an increase in the RMSE (and MSLL) was observed as more measurement data from different magnetometers was combined.

Possible explanations why the magnetic field model using a subset of magnetometers with similar altitudes does not yield a decrease in RMSE and MSLL, compared to the case where the data of the magnetometers are used individually, are discussed in Chapter 4. It is expected that possible explanations are either that the magnetometer calibration failed, or that the assumption that the magnetometers coincide with the magnetometer locations was not valid, or that the influence of the walls prohibited successful magnetic field mapping using multiple magnetometers.

The benefits of the MOCAP suit are that it is equipped with seventeen high quality magnetometers and that it accurately determines the locations of the body segments in a navigation coordinate frame, especially regarding the altitudes. The challenges on the other hand are related to making a 3D magnetic field map with multiple magnetometers from the suit. The hypothesis was that using multiple magnetometers operating at approximately the same altitude would improve the quality of the magnetic field map compared to the scenario where either a single magnetometer or all magnetometers at once were used. Surprisingly, this hypothesis was not supported during the experiments. Increasing the amount of magnetometers in the subset resulted in an increase of the RMSE and the MSLL of the predictions. Since magnetometers at similar altitudes should observe a magnetic field with similar characteristics, it is not expected that combining measurements from multiple magnetometers operating at similar altitudes cannot improve the magnetic field map quality. Instead, it is expected that an other problem occurred. Potentially the calibration of the magnetometers was erroneous or the assumption that the magnetometer measurements came from the body segment locations is not valid.

For future work it is recommended to examine if each magnetometer returns identical outputs when placed at identical locations, where also the orientation of each magnetometer must be considered. Moreover, it is suggested to focus on combining measurements from multiple magnetometers at similar altitudes. It is believed that the contact detection in combination with the biomechanical model of the MOCAP suit is a promising feature for magnetic field mapping, considering the observation that the magnetic field in indoor environments varies with altitude. Possibly SLAM can play a role in accurately determining the absolute magnetometer positions.

Appendix A

Body dimensions for the motion capture suit

Table A-1 shows the body dimensions that are included to enhance the calibration of the body segments from the Xsens MVN Link MOCAP suit.

Body dimension	Length [cm]
Body height	194
Foot or shoe length	30
Shoulder height	168
Shoulder width	45
Elbow span	97
Wrist span	148
Arm span	195
Hip height	111
Hip width	27
Knee height	59
Extra shoe sole thickness	0

Table A-1: Body dimensions of the user wearing the Xsens MVN Link MOCAP suit.

Appendix B

Additional results

This appendix provides the figures and tables for the moving methods which are not shown in the report. Appendix B-1 contains the contour plots for determining the hyperparameters. Appendix B-2 contains the tables with magnetometer mean heights and hyperparameters. Appendix B-3 contains the contour plots of the reduced-rank GPR for the single magnetometers are shown. Lastly, the MSLL metrics for the combinations of magnetometers are presented in Appendix B-4. The two trajectories which are evaluated are trajectory A which starts along the x_1-direction and trajectory B which starts along the x_2-direction.

B-1 Contour plots

B-1-1 Standard moving for trajectory B

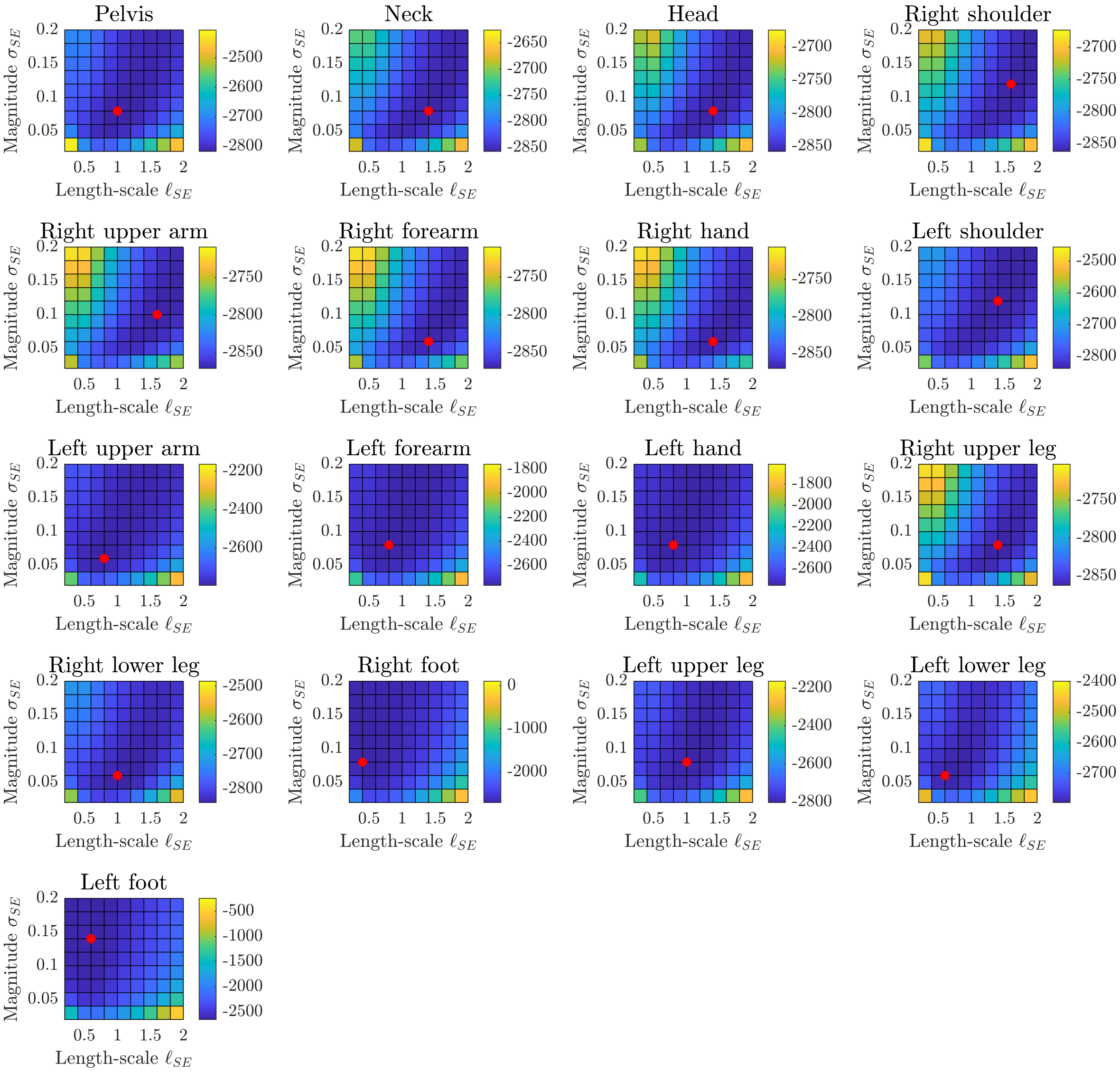

Figure B-1: The NLML evaluated for different length-scale ℓ_{SE} [m] and magnitude hyperparameter σ_{SE} [-] pairs with the data from trajectory B1: standard walking. The optimal pair is indicated by a red dot.

B-1-2 T-pose moving for trajectory A

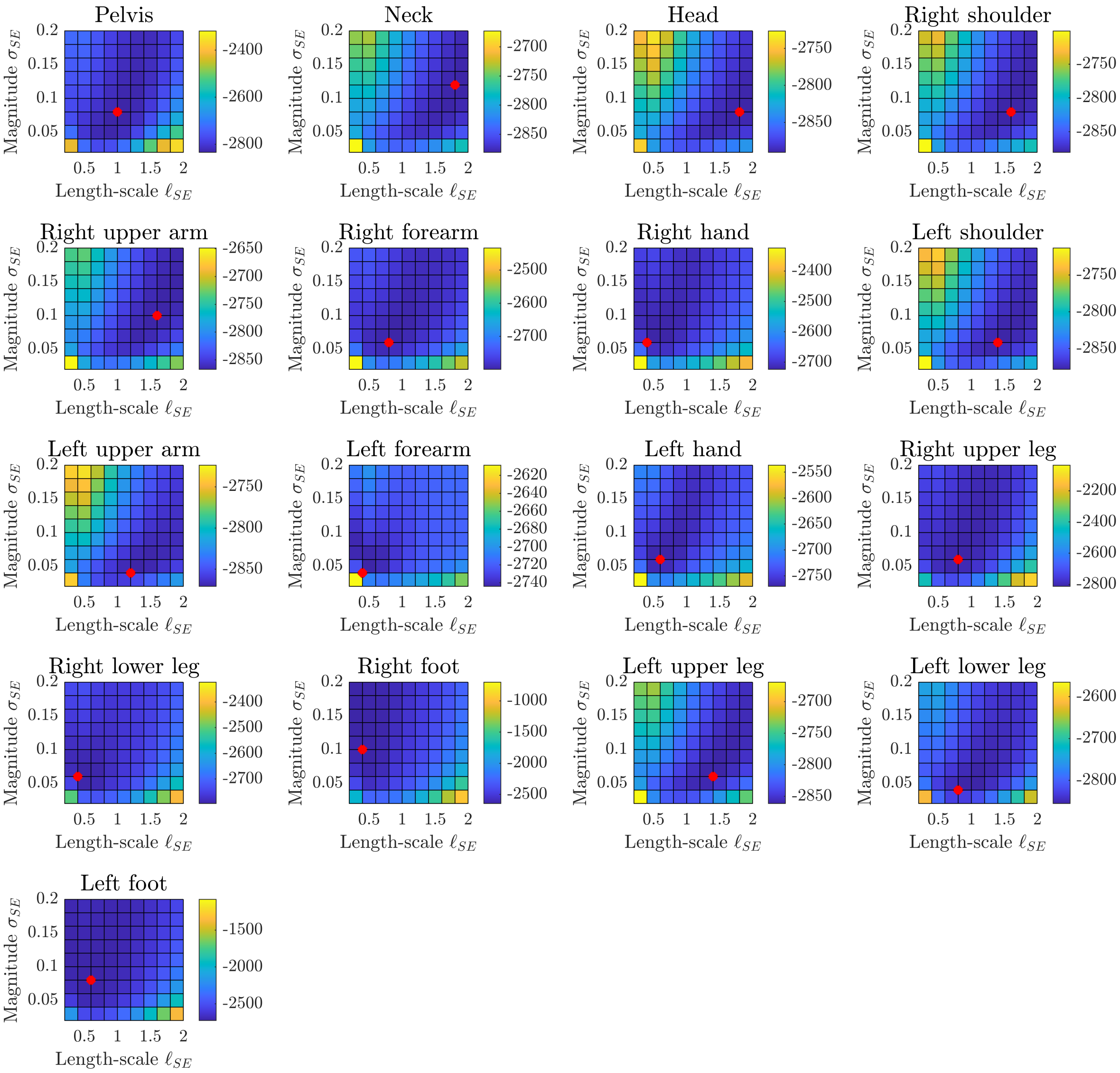

Figure B-2: The NLML evaluated for different length-scale ℓ_{SE} [m] and magnitude hyperparameter σ_{SE} [-] pairs with the data from trajectory A2: T-pose walking. The optimal pair is indicated by a red dot.

B-1-3 T-pose moving for trajectory B

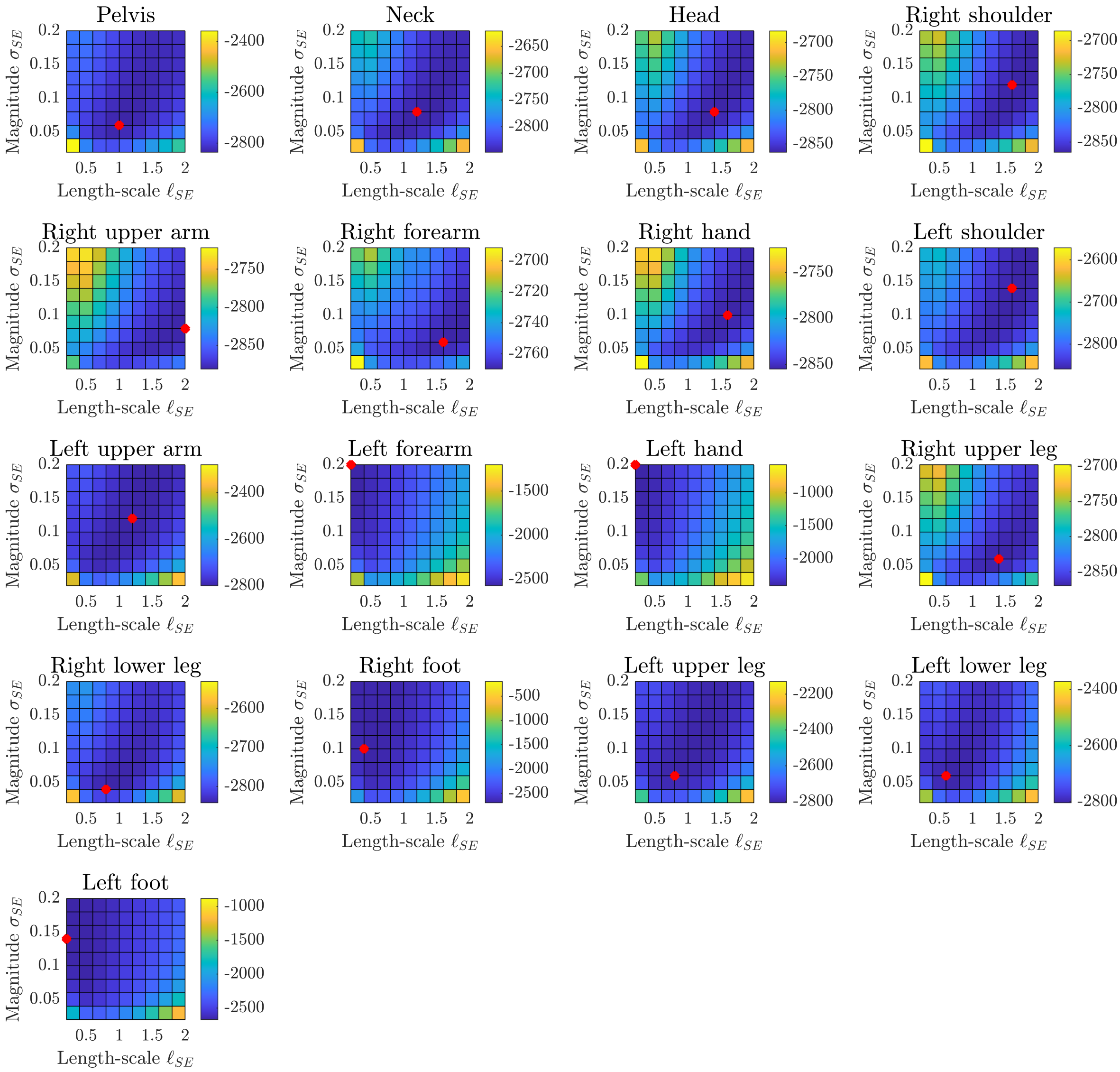

Figure B-3: The NLML evaluated for different length-scale ℓ_{SE} [m] and magnitude hyperparameter σ_{SE} [-] pairs with the data from trajectory B2: T-pose walking. The optimal pair is indicated by a red dot.

The optimal hyperparameters for the measurement data of three of the magnetometers exceed the maximum domain. Therefore, the NLML is evaluated again for a different range, such that a minimum appears. The figures are shown below.

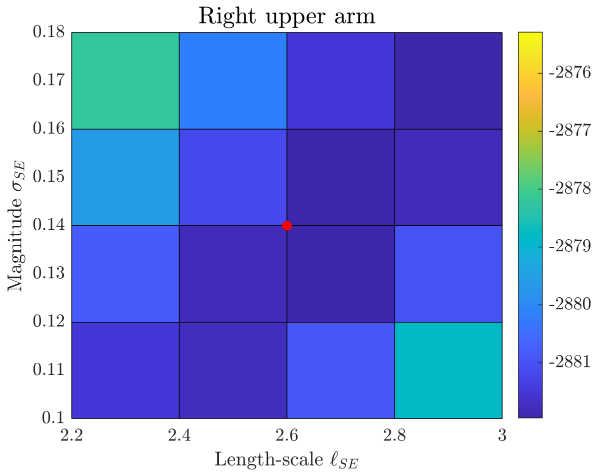

Figure B-4: NLML minimum for the RUA magnetometer, with ℓ_{SE} [m] and σ_{SE} [-].

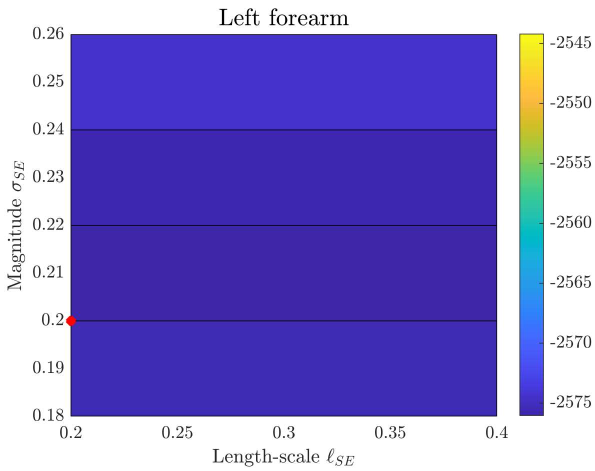

Figure B-5: NLML minimum for the LFA magnetometer, with ℓ_{SE} [m] and σ_{SE} [-].

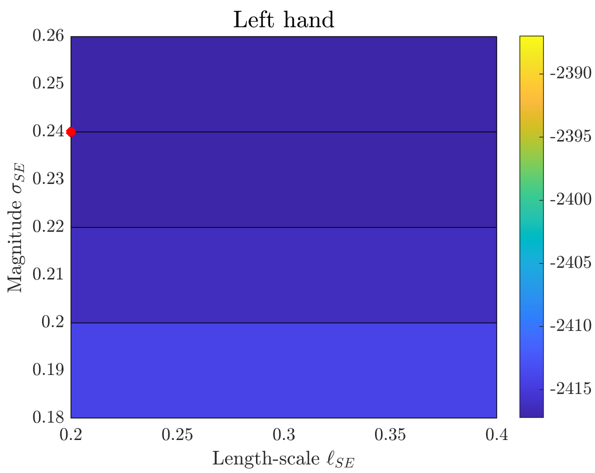

Figure B-6: NLML minimum for the LH magnetometer, with ℓ_{SE} [m] and σ_{SE} [-].

B-1-4 Frog-like moving for trajectory A

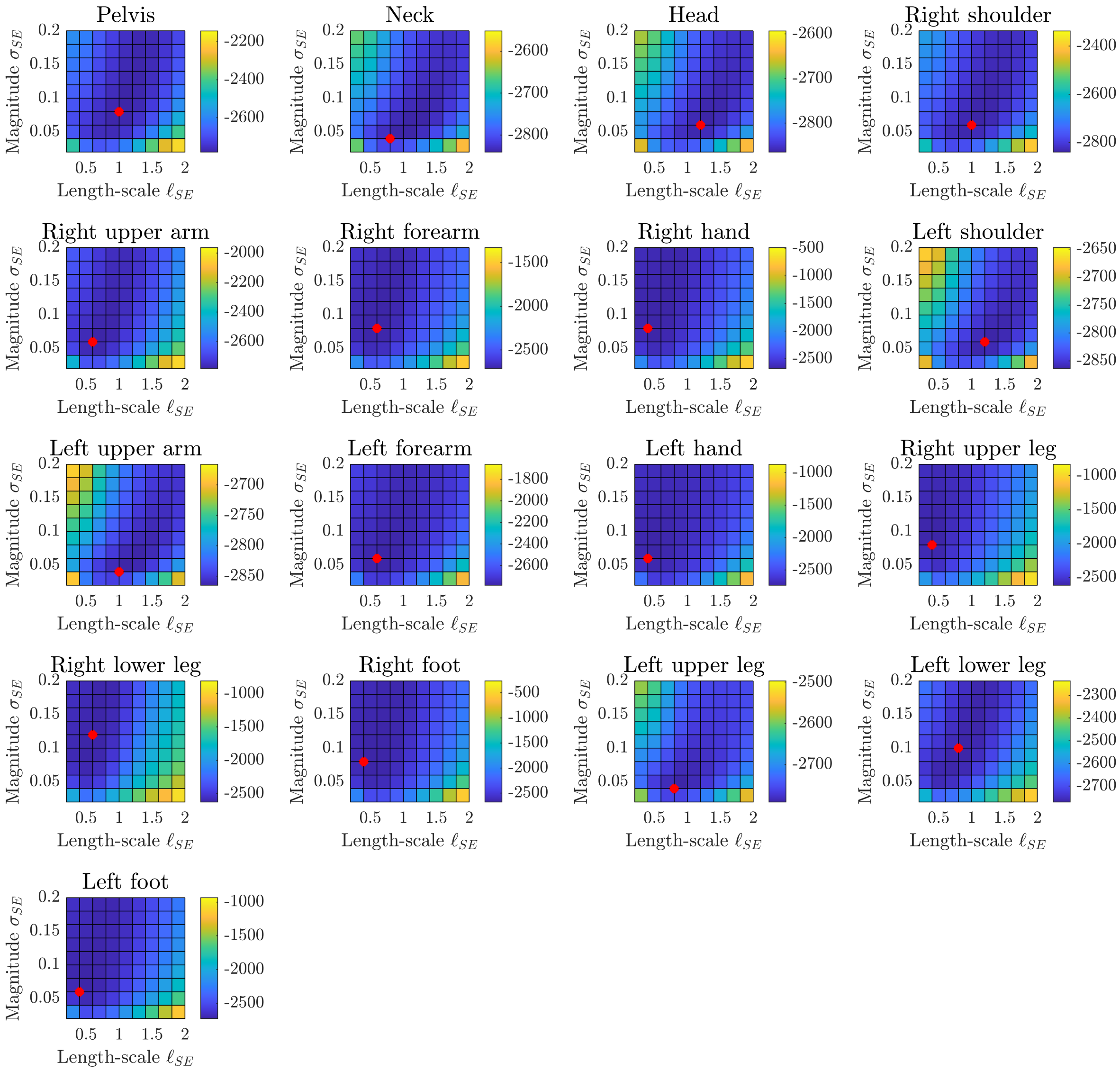

Figure B-7: The NLML evaluated for different length-scale ℓ_{SE} [m] and magnitude hyperparameter σ_{SE} [-] pairs with the data from trajectory A3: frog-like walking. The optimal pair is indicated by a red dot.

B-1-5 Frog-like moving for trajectory B

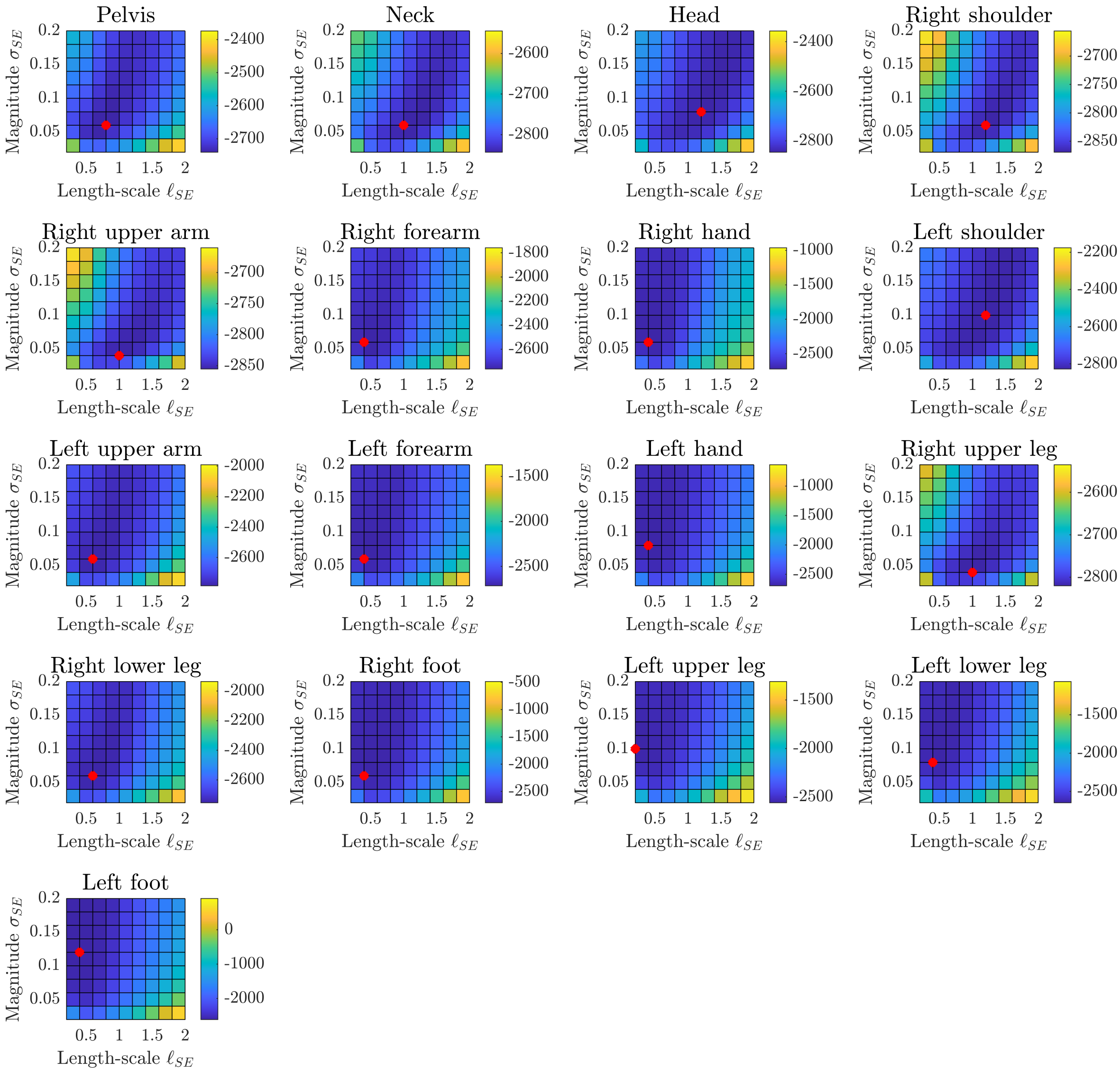

Figure B-8: The NLML evaluated for different length-scale ℓ_{SE} [m] and magnitude hyperparameter σ_{SE} [-] pairs with the data from trajectory B3: frog-like walking. The optimal pair is indicated by a red dot.

B-1-6 Arms-high moving for trajectory A

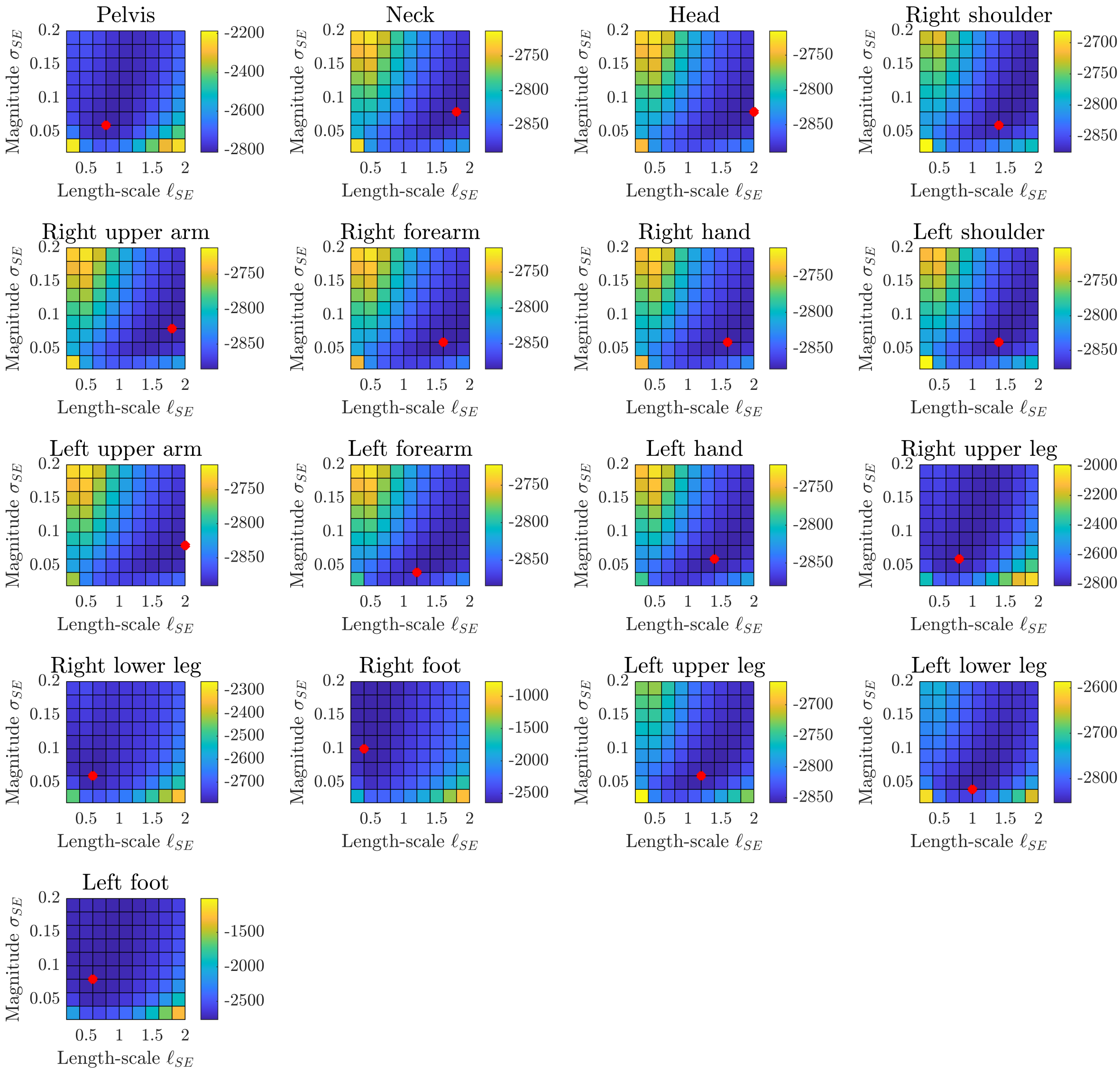

Figure B-9: The NLML evaluated for different length-scale ℓ_{SE} [m] and magnitude hyperparameter σ_{SE} [-] pairs with the data from trajectory A4: arms-high walking. The optimal pair is indicated by a red dot.

The optimal hyperparameters for the measurement data of three of the magnetometers exceed the maximum domain. Therefore, the NLML is evaluated again for a different range, such that a minimum appears. The figures are shown below.

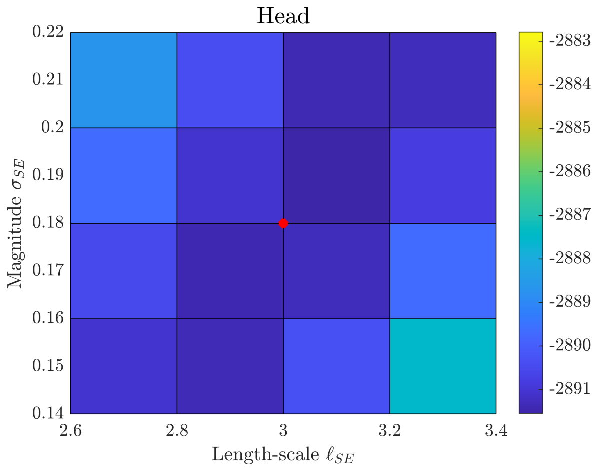

Figure B-10: NLML minimum for the H magnetometer, with ℓ_{SE} [m] and σ_{SE} [-].

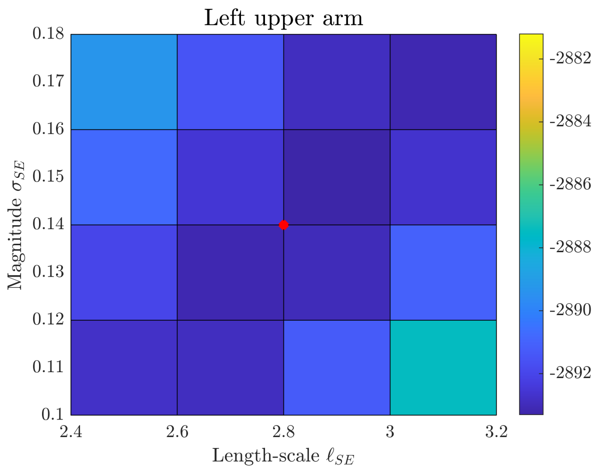

Figure B-11: NLML minimum for the LUA magnetometer, with ℓ_{SE} [m] and σ_{SE} [-].

B-1-7 Arms-high moving for trajectory B

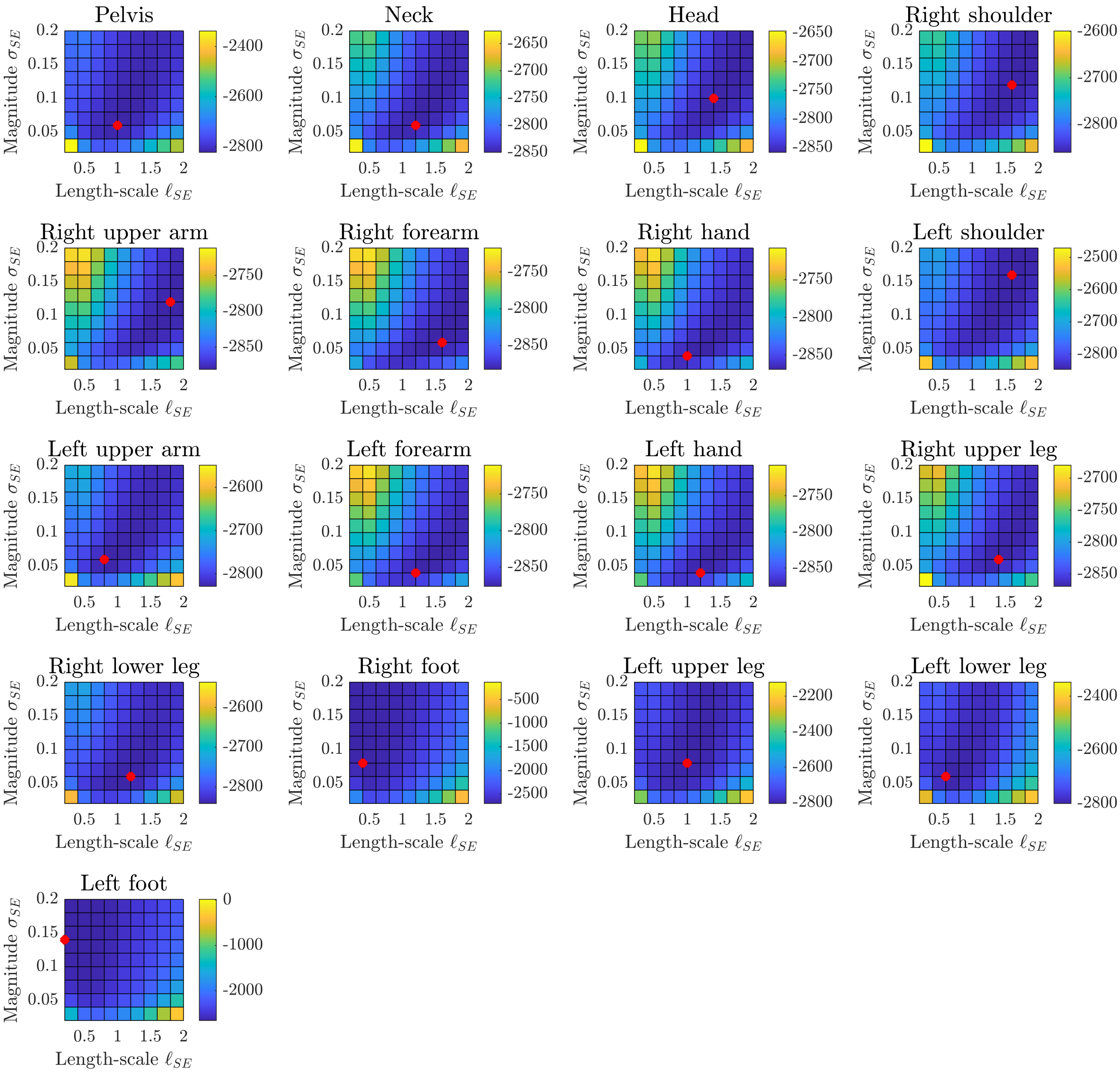

Figure B-12: The NLML evaluated for different length-scale ℓ_{SE} [m] and magnitude hyperparameter σ_{SE} [-] pairs with the data from trajectory B4: arms-high walking. The optimal pair is indicated by a red dot.

B-2 Tables with magnetometer mean heights and hyperparameters

B-2-1 T-pose walk: heights and hyperparameters

	Trajectory A2				Trajectory B2			
Magnetometer position	Mean height [m]	Height std. dev. [m]	ℓ_{SE}	σ_{SE}	Mean height [m]	Height std. dev. [m]	ℓ_{SE}	σ_{SE}
Head	1.730	0.032	1.8	0.08	1.738	0.034	1.4	0.08
RUA	1.598	0.033	1.6	0.10	1.608	0.034	2.6	0.14
LUA	1.590	0.034	1.2	0.04	1.605	0.036	1.2	0.12
RS	1.586	0.032	1.6	0.08	1.594	0.034	1.6	0.12
LS	1.585	0.032	1.4	0.06	1.594	0.034	1.6	0.14
RFA	1.532	0.036	0.8	0.06	1.555	0.038	1.6	0.06
LFA	1.509	0.042	0.4	0.04	1.512	0.069	0.2	0.20
Neck	1.506	0.032	1.8	0.12	1.514	0.034	1.2	0.08
RH	1.441	0.050	0.4	0.06	1.472	0.050	1.6	0.10
LH	1.426	0.054	0.6	0.06	1.459	0.070	0.2	0.24
LUL	1.095	0.032	1.4	0.06	1.104	0.035	0.8	0.06
RUL	1.091	0.032	0.8	0.06	1.096	0.033	1.4	0.06
Pelvis	1.092	0.032	1.0	0.08	1.099	0.034	1.0	0.06
LLL	0.583	0.023	0.8	0.04	0.593	0.022	0.6	0.06
RLL	0.572	0.028	0.8	0.06	0.579	0.027	1.4	0.06
LF	0.156	0.059	0.6	0.08	0.164	0.057	0.2	0.02
RF	0.150	0.057	0.4	0.10	0.156	0.059	0.4	0.10

Table B-1: Mean magnetometer heights and standard deviation of magnetometers and optimal hyperparameters based on contour plots for both T-pose walking trajectories A2 and B2.

B-2-2 Frog walk: heights and hyperparameters

	Trajectory A3				Trajectory B3			
Magnetometer position	Mean height [m]	Height std. dev. [m]	ℓ_{SE}	σ_{SE}	Mean height [m]	Height std. dev. [m]	ℓ_{SE}	σ_{SE}
Head	0.805	0.045	1.2	0.06	0.772	0.051	1.2	0.08
RS	0.792	0.050	1.0	0.06	0.758	0.056	1.2	0.06
LS	0.796	0.047	1.2	0.06	0.764	0.053	1.2	0.10
RUA	0.731	0.053	0.6	0.06	0.689	0.060	1.0	0.04
LUA	0.779	0.045	1.0	0.04	0.749	0.046	0.6	0.06
Neck	0.775	0.055	0.8	0.04	0.743	0.061	1.0	0.06
LUL	0.556	0.107	0.8	0.04	0.527	0.112	0.2	0.10
RUL	0.533	0.016	0.4	0.08	0.504	0.112	1.0	0.04
Pelvis	0.543	0.106	1.0	0.08	0.514	0.112	0.8	0.06
RFA	0.454	0.050	0.6	0.08	0.413	0.056	0.4	0.06
LFA	0.497	0.045	0.6	0.06	0.467	0.046	0.4	0.06
LLL	0.360	0.102	0.8	0.10	0.357	0.101	0.4	0.08
RLL	0.307	0.127	0.6	0.12	0.307	0.120	0.6	0.06
RH	0.215	0.050	0.4	0.08	0.175	0.056	0.4	0.06
LH	0.253	0.046	0.4	0.06	0.227	0.045	0.4	0.08
LF	0.192	0.026	0.4	0.06	0.196	0.027	0.4	0.12
RF	0.170	0.037	0.4	0.08	0.174	0.035	0.4	0.06

Table B-2: Mean magnetometer heights and standard deviation of magnetometers and optimal hyperparameters based on contour plots for both frog-like walking trajectories A3 and B3.

B-2-3 Arms high walk: heights and hyperparameters

	Trajectory A4				Trajectory B4			
Magnetometer position	Mean height [m]	Height std. dev. [m]	ℓ_{SE}	σ_{SE}	Mean height [m]	Height std. dev. [m]	ℓ_{SE}	σ_{SE}
RH	2.096	0.065	1.6	0.06	2.065	0.046	1.0	0.04
LH	2.095	0.062	1.4	0.06	2.034	0.045	1.2	0.04
RFA	1.877	0.045	1.6	0.06	1.851	0.041	1.6	0.06
LFA	1.874	0.044	1.2	0.04	1.840	0.039	1.2	0.04
Head	1.737	0.033	3.0	0.18	1.738	0.038	1.4	0.10
RUA	1.630	0.034	1.8	0.08	1.620	0.038	1.8	0.12
LUA	1.633	0.035	2.8	0.14	1.622	0.040	0.8	0.06
RS	1.589	0.033	1.4	0.06	1.590	0.038	1.6	0.12
LS	1.589	0.033	1.4	0.06	1.589	0.038	1.6	0.16
Neck	1.510	0.033	1.8	0.08	1.510	0.038	1.2	0.06
LUL	1.102	0.033	1.2	0.06	1.102	0.037	1.0	0.08
RUL	1.094	0.032	0.8	0.06	1.093	0.037	1.4	0.06
Pelvis	1.097	0.032	0.8	0.06	1.096	0.037	1.0	0.06
LLL	0.591	0.022	1.0	0.04	0.600	0.020	0.6	0.06
RLL	0.578	0.024	0.6	0.06	0.574	0.030	1.2	0.06
LF	0.161	0.055	0.6	0.08	0.162	0.051	0.2	0.14
RF	0.150	0.055	0.4	0.10	0.157	0.057	0.4	0.08

Table B-3: Mean magnetometer heights and standard deviation of magnetometers and optimal hyperparameters based on contour plots for both arms-high walking trajectories A4 and B4.

B-3 Single magnetometer GPR

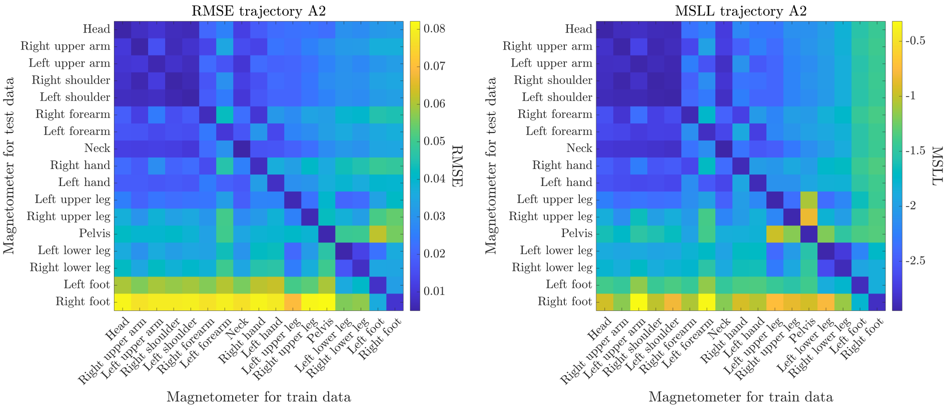

Figure B-13: The performance metrics for the T-pose walking experiment for trajectory A2 where data from a single magnetometer is used to make predictions at all magnetometer locations.

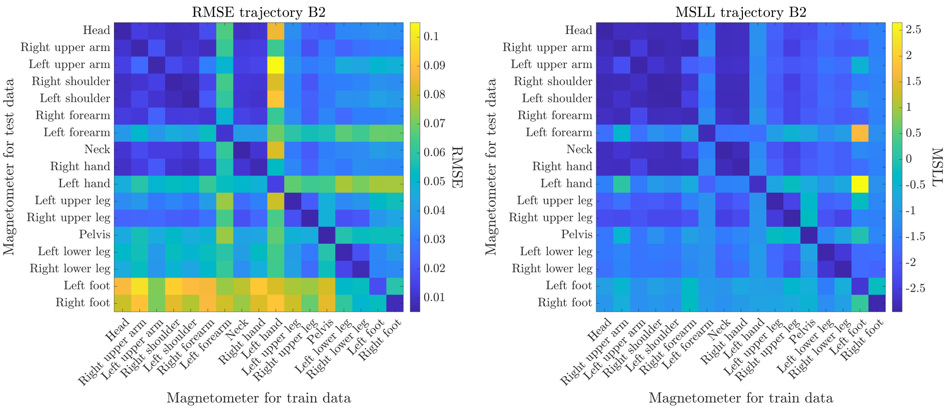

Figure B-14: The performance metrics for the T-pose walking experiment for trajectory B2 where data from a single magnetometer is used to make predictions at all magnetometer locations.

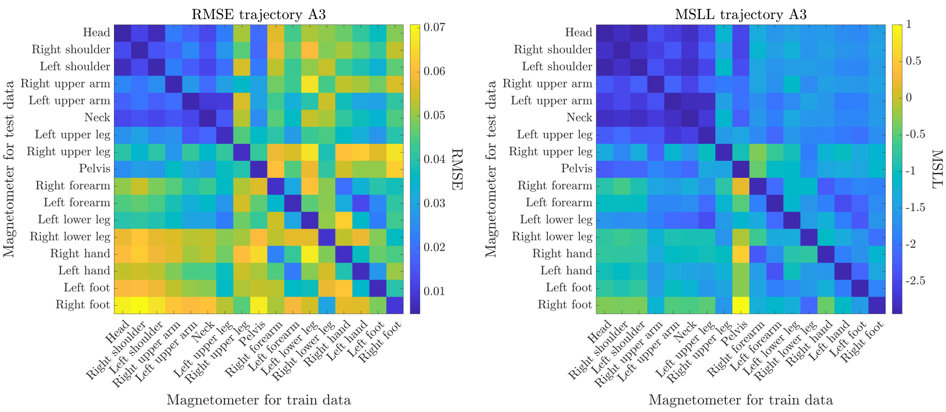

Figure B-15: The performance metrics for the frog-like walking experiment for trajectory A3 where data from a single magnetometer is used to make predictions at all magnetometer locations.

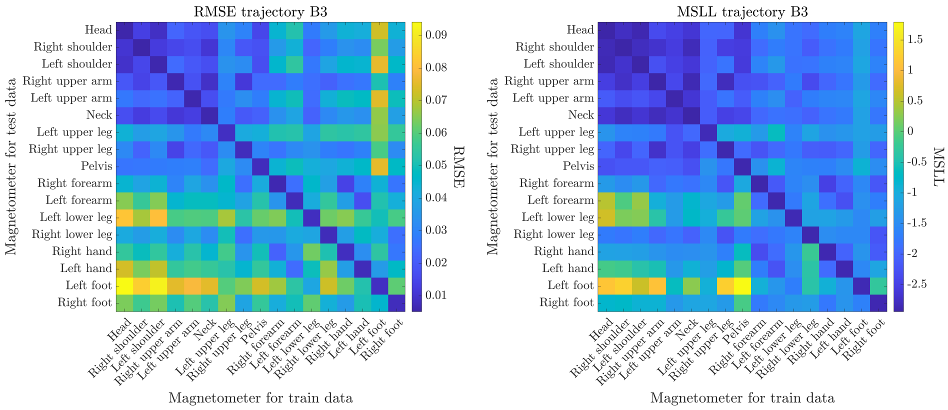

Figure B-16: The performance metrics for the frog-like walking experiment for trajectory B3 where data from a single magnetometer is used to make predictions at all magnetometer locations.

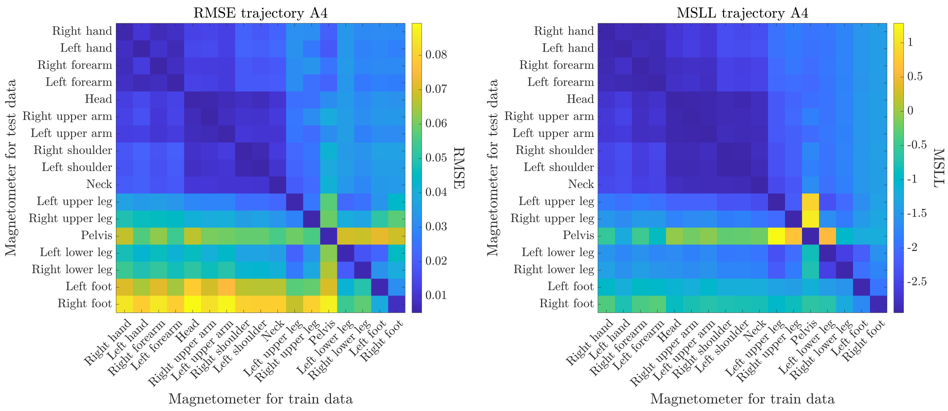

Figure B-17: The performance metrics for the arms-high walking experiment for trajectory A4 where data from a single magnetometer is used to make predictions at all magnetometer locations.

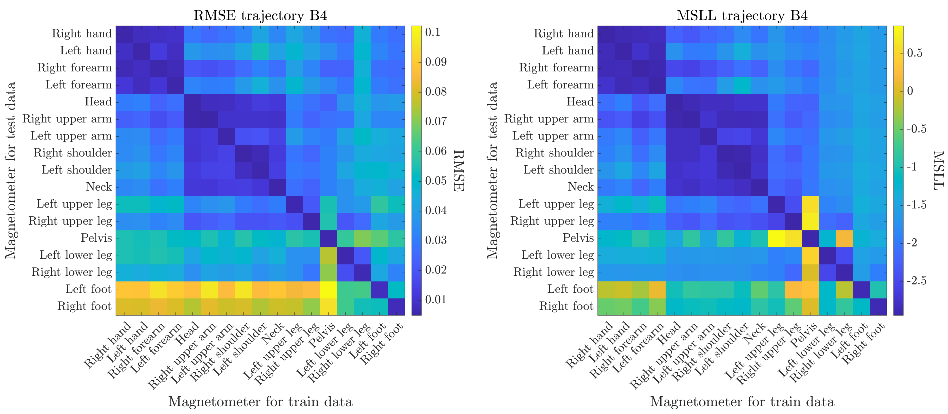

Figure B-18: The performance metrics for the arms-high walking experiment for trajectory B4 where data from a single magnetometer is used to make predictions at all magnetometer locations.

B-4 MSLL Combinations

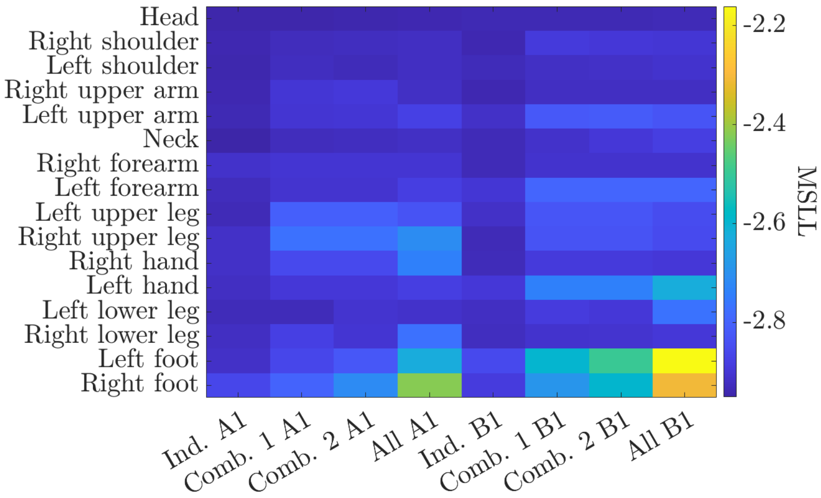

Figure B-19: Comparison of the MSLL of the different magnetometer combinations for the standard moving method along trajectory A and B.

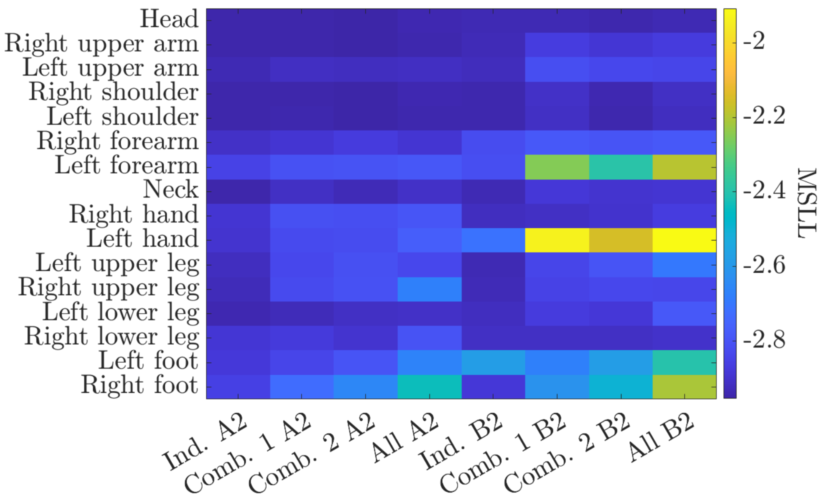

Figure B-20: Comparison of the MSLL of the different magnetometer combinations for the T-pose moving method along trajectory A and B.

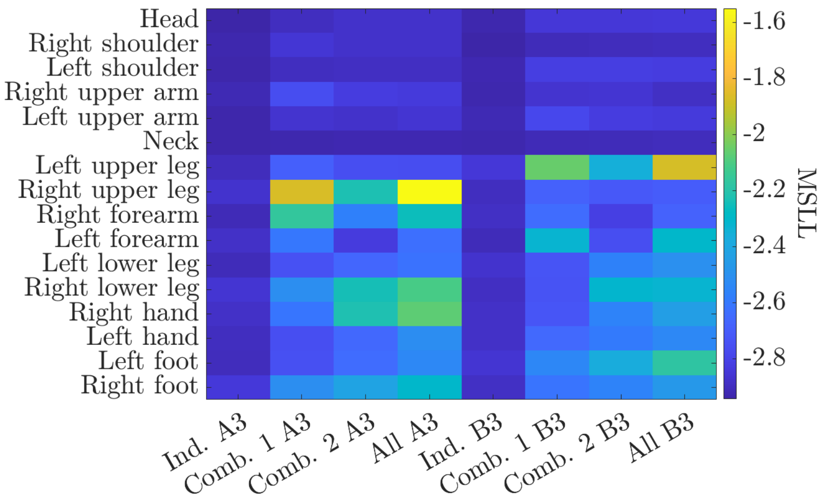

Figure B-21: Comparison of the MSLL of the different magnetometer combinations for the frog-like moving method along trajectory A and B.

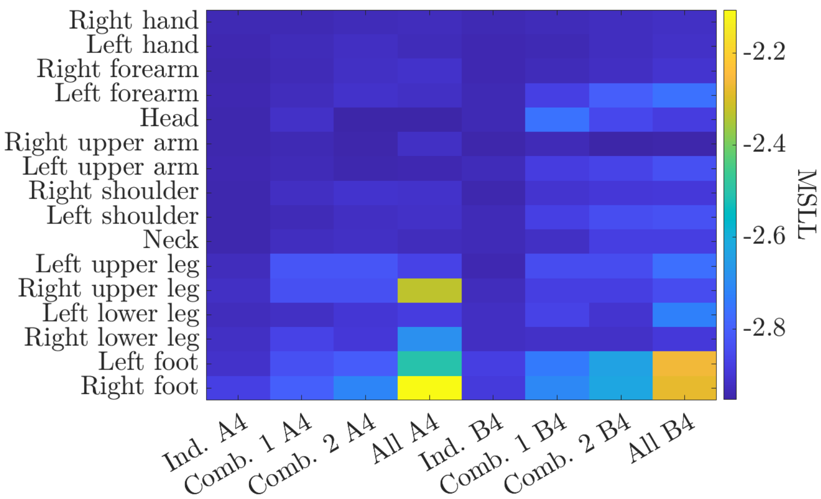

Figure B-22: Comparison of the MSLL of the different magnetometer combinations for the arms-high moving method along trajectory A and B.

Bibliography

[1] A. Solin, S. Särkkä, J. Kannala, and E. Rahtu, "Terrain navigation in the magnetic landscape: Particle filtering for indoor positioning," in *Proceedings of the 2016 European Navigation Conference (ENC)*, pp. 1–9, 2016.

[2] P. Puricer and P. Kovar, "Technical limitations of GNSS receivers in indoor positioning," in *Proceedings of the 2007 17th International Conference Radioelektronika*, pp. 1–5, 2007.

[3] E. Dorveaux, T. Boudot, M. Hillion, and N. Petit, "Combining inertial measurements and distributed magnetometry for motion estimation," in *Proceedings of the 2011 American Control Conference*, pp. 4249–4256, 2011.

[4] D. Vissière, A. Martin, and N. Petit, "Using magnetic disturbances to improve IMU-based position estimation," in *Proceedings of the 2007 European Control Conference (ECC)*, pp. 2853–2858, 2007.

[5] B. Li, T. Gallagher, A. G. Dempster, and C. Rizos, "How feasible is the use of magnetic field alone for indoor positioning?," in *Proceedings of the 2012 International Conference on Indoor Positioning and Indoor Navigation (IPIN)*, pp. 1–9, 2012.

[6] N. Wahlström, M. Kok, T. B. Schön, and F. Gustafsson, "Modeling magnetic fields using Gaussian processes," in *Proceedings of the 2013 IEEE International Conference on Acoustics, Speech and Signal Processing*, pp. 3522–3526, 2013.

[7] E. Le Grand and S. Thrun, "3-axis magnetic field mapping and fusion for indoor localization," in *Proceedings of the 2012 IEEE International Conference on Multisensor Fusion and Integration for Intelligent Systems (MFI)*, pp. 358–364, 2012.

[8] M. Angermann, M. Frassl, M. Doniec, B. J. Julian, and P. Robertson, "Characterization of the indoor magnetic field for applications in localization and mapping," in *Proceedings of the 2012 International Conference on Indoor Positioning and Indoor Navigation (IPIN)*, pp. 1–9, 2012.

[9] W. Storms, J. Shockley, and J. Raquet, “Magnetic field navigation in an indoor environment,” in *Proceedings of the 2010 Ubiquitous Positioning Indoor Navigation and Location Based Service*, pp. 1–10, 2010.

[10] I. Skog, “Inertial and magnetic-field sensor arrays - capabilities and challenges,” in *Proceedings of the 2018 IEEE SENSORS*, pp. 1–4, 2018.

[11] T. Edridge and M. Kok, “Mapping the magnetic field using a magnetometer array with noisy input Gaussian process regression,” in *Proceedings of the 2023 26th International Conference on Information Fusion (FUSION)*, pp. 1–7, 2023.

[12] I. Skog, J. Jaldén, J.-O. Nilsson, and F. Gustafsson, “Position and orientation estimation of a permanent magnet using a small-scale sensor array,” in *Proceedings of the 2018 IEEE International Instrumentation and Measurement Technology Conference (I2MTC)*, pp. 1–5, 2018.

[13] I. Skog, G. Hendeby, and F. Gustafsson, “Magnetic odometry - a model-based approach using a sensor array,” in *Proceedings of the 2018 21st International Conference on Information Fusion (FUSION)*, pp. 794–798, 2018.

[14] C. Huang, G. Hendeby, and I. Skog, “A tightly-integrated magnetic-field aided inertial navigation system,” in *Proceedings of the 2022 25th International Conference on Information Fusion (FUSION)*, pp. 1–8, 2022.

[15] I. Skog, G. Hendeby, and F. Trulsson, “Magnetic-field based odometry – an optical flow inspired approach,” in *Proceedings of the 2021 International Conference on Indoor Positioning and Indoor Navigation (IPIN)*, pp. 1–8, 2021.

[16] D. Hanley, A. S. D. d. Oliveira, X. Zhang, D. H. Kim, Y. Wei, and T. Bretl, “The impact of height on indoor positioning with magnetic fields,” *IEEE Transactions on Instrumentation and Measurement*, vol. 70, pp. 1–19, 2021.

[17] D. Roetenberg, H. Luinge, and P. J. Slycke, “Xsens MVN: Full 6DOF human motion tracking using miniature inertial sensors,” 2009.

[18] A. Solin, M. Kok, N. Wahlström, T. B. Schön, and S. Särkkä, “Modeling and interpolation of the ambient magnetic field by Gaussian processes,” *IEEE Transactions on Robotics*, vol. 34, no. 4, pp. 1112–1127, 2018.

[19] F. Zafari, A. Gkelias, and K. K. Leung, “A survey of indoor localization systems and technologies,” *IEEE Communications Surveys Tutorials*, vol. 21, no. 3, pp. 2568–2599, 2019.

[20] C. Debeunne and D. Vivet, “A review of visual-lidar fusion based simultaneous localization and mapping,” *Sensors*, vol. 20, no. 7, 2020.

[21] O. J. Woodman, “An introduction to inertial navigation,” Tech. Rep. UCAM-CL-TR-696, University of Cambridge, Computer Laboratory, Aug. 2007.

[22] F. Viset, J. T. Gravdahl, and M. Kok, “Magnetic field norm SLAM using Gaussian process regression in foot-mounted sensors,” in *Proceedings of the 2021 European Control Conference (ECC)*, pp. 392–398, 2021.

[23] M. Kok and A. Solin, "Scalable magnetic field SLAM in 3D using Gaussian process maps," in *Proceedings of the 2018 21st International Conference on Information Fusion (FUSION)*, pp. 1353–1360, 2018.

[24] I. Vallivaara, J. Haverinen, A. Kemppainen, and J. Röning, "Simultaneous localization and mapping using ambient magnetic field," in *Proceedings of the 2010 IEEE Conference on Multisensor Fusion and Integration*, pp. 14–19, 2010.

[25] P. Robertson, M. Frassl, M. Angermann, M. Doniec, B. J. Julian, M. Garcia Puyol, M. Khider, M. Lichtenstern, and L. Bruno, "Simultaneous localization and mapping for pedestrians using distortions of the local magnetic field intensity in large indoor environments," in *Proceedings of the International Conference on Indoor Positioning and Indoor Navigation*, pp. 1–10, 2013.

[26] S. He and K. G. Shin, "Geomagnetism for smartphone-based indoor localization: Challenges, advances, and comparisons," *ACM Comput. Surv.*, vol. 50, Dec. 2017.

[27] J. Haverinen and A. Kemppainen, "Global indoor self-localization based on the ambient magnetic field," *Robotics and Autonomous Systems*, vol. 57, no. 10, pp. 1028–1035, 2009. Proceedings of the 5th International Conference on Computational Intelligence, Robotics and Autonomous Systems (5th CIRAS).

[28] M. Kok and A. Solin, "Scalable magnetic field SLAM in 3D using Gaussian process maps," in *Proceedings of the 2018 21st International Conference on Information Fusion (FUSION)*, pp. 1353–1360, 2018.

[29] N. Akai and K. Ozaki, "3D magnetic field mapping in large-scale indoor environment using measurement robot and Gaussian processes," in *Proceedings of the 2017 International Conference on Indoor Positioning and Indoor Navigation (IPIN)*, pp. 1–7, 2017.

[30] M. Kok and T. B. Schön, "Magnetometer calibration using inertial sensors," *IEEE Sensors Journal*, vol. 16, no. 14, pp. 5679–5689, 2016.

[31] D. Gebre-Egziabher, G. H. Elkaim, J. D. Powell, and B. W. Parkinson, "Calibration of strapdown magnetometers in magnetic field domain," *Journal of Aerospace Engineering*, vol. 19, no. 2, pp. 87–102, 2006.

[32] J. F. Vasconcelos, G. Elkaim, C. Silvestre, P. Oliveira, and B. Cardeira, "Geometric approach to strapdown magnetometer calibration in sensor frame," *IEEE Transactions on Aerospace and Electronic Systems*, vol. 47, no. 2, pp. 1293–1306, 2011.

[33] V. Renaudin, M. Afzal, and G. Lachapelle, "Complete triaxis magnetometer calibration in the magnetic domain," *Journal of Sensors*, 2010.

[34] Y. Wu and W. Shi, "On calibration of three-axis magnetometer," *IEEE Sensors Journal*, vol. 15, no. 11, pp. 6424–6431, 2015.

[35] C. Rasmussen and C. Williams, *Gaussian Processes for Machine Learning.* The MIT Press, 2006.

[36] H.-S. Kim, W. Seo, and K.-R. Baek, "Indoor positioning system using magnetic field map navigation and an encoder system," *Sensors*, vol. 17, no. 3, 2017.

[37] F. Viset, R. Helmons, and M. Kok, "Distributed multi-agent magnetic field norm SLAM with gaussian processes," in *Proceedings of the 2023 26th International Conference on Information Fusion (FUSION)*, pp. 1–8, 2023.

[38] T. Veen, "Magnetic field SLAM using an inertial human motion suit and reduced rank Gaussian process," Master's thesis, TU Delft, 2022.

[39] C. Menzen, M. Fetter, and M. Kok, "Large-scale magnetic field maps using structured kernel interpolation for gaussian process regression," in *Proceedings of the 2023 26th International Conference on Information Fusion (FUSION)*, pp. 1–7, 2023.

[40] F. Viset, R. Helmons, and M. Kok, "Distributed multi-agent magnetic field norm SLAM with Gaussian processes," in *Proceedings of the 2023 26th International Conference on Information Fusion (FUSION)*, pp. 1–8, 2023.

[41] F. Viset, R. Helmons, and M. Kok, "An extended kalman filter for magnetic field SLAM using Gaussian process regression," *Sensors*, vol. 22(8):2833, 2022.

[42] A. McHutchon, *Nonlinear Modelling and Control using Gaussian Processes*. PhD thesis, University of Cambridge, 2014.

[43] A. Solin and S. Särkkä, "Hilbert space methods for reduced-rank Gaussian process regression," *Statistics and Computing*, vol. 30, p. 419–446, Aug. 2019.

[44] Xsens, *Xsens MVN User Manual*, November 2017.

[45] Xsens, *Magnetic Calibration Manual*, November 2019.

Glossary

List of Acronyms

BFGS	Broyden-Fletcher-Goldfarb-Shanno
GNSS	global navigation satellite system
GP	Gaussian process
GPR	Gaussian process regression
i.i.d.	independent and identically distributed
INS	inertial navigation system
IMU	inertial measurement unit
LiDAR	Light Detection and Ranging
MEMS	micro-electro-mechanical systems
MOCAP	motion capture
NLML	negative log marginal likelihood
RMSE	root mean squared error
SE	squared-exponential
SLAM	simultaneous localization and mapping
MSLL	mean standardized log loss
ZMWN	zero-mean white noise
ZUPT-aided EKF	zero velocity update-aided extended Kalman filter
P	pelvis
N	neck
H	head
RS	right shoulder
RUA	right upper arm
RFA	right forearm

RH	right hand
LS	left shoulder
LUA	left upper arm
LFA	left forearm
LH	left hand
RUL	right upper leg
RLL	right lower leg
RF	right foot
LUL	left upper leg
LLL	left lower leg
LF	left foot